Quantifying importance of macrobenthos for benthic-pelagic coupling in a temperate coastal shelf sea

Wenyan Zhang [1,*] Andreas Neumann[1], Ute Daewel[1], Kai Wirtz[1], Justus E.E. van Beusekom[1], Annika Eisele[1], Mengyao Ma[1] and Corinna Schrum[1,2]

[1] Institute of Coastal Research, Helmholtz-Zentrum Geesthacht, Geesthacht, 21502, Germany
[2] Institute of Oceanography, Center for Earth System Research and Sustainability, University of Hamburg, Hamburg, 20146, Germany

[*] Correspondence to: Wenyan Zhang (wenyan.zhang@hzg.de)

Key Points:

- A novel 3D numerical model resolves interactions among macrobenthos, bioturbation, oxygen consumption and carbon early diagenesis
- The role of bioturbation in benthic oxygen consumption is twofold and dependent on sediment properties and hydrodynamics
- Bioturbation-induced oxygen consumption contributes to more than 52% of the total benthic oxygen fluxes at a regional scale

Abstract

Benthic oxygen fluxes consist of advective and diffusive terms. Both terms in the south-eastern North Sea exhibit a prominent annual cycle but with opposite variation patterns. To understand the driving mechanisms quantitatively, a novel 3-D benthic-pelagic coupled model resolving interactions among macrobenthos, bioturbation, oxygen consumption and carbon early diagenesis was applied to reconstruct the benthic states. Simulation results show a satisfactory agreement with field data and reveal that the benthic oxygen flux is determined by not only pelagic drivers but also by internal dynamics associated with the interaction between organic carbon and macrobenthos, and bedform morphodynamics. Variation of advective flux, characterized by summer-low and winter-high, is mainly driven by

hydrodynamics and bedform morphodynamics, while variation of diffusive flux, featured by summer-high and winter-low, is a compound effect of pelagic and benthic drivers with a dominant control by macrobenthos through bioturbation. The role of bioturbation in benthic oxygen consumption is twofold: (i) on the one hand, it alters the particulate organic carbon (POC) distribution in surface sediments, thereby changing the availability of POC to oxygen consumption; (ii) on the other hand, it mixes oxygen down into sediments, thereby facilitating oxygen consumption. Our results indicate that the first role prevails in sandy seafloor characterized by energetic hydrodynamics, while the second role becomes increasingly important along with a weakening of bottom currents. We found that bioturbation-induced oxygen consumption contributes to more than 85% and 52% of the total benthic oxygen fluxes in muddy seabed and at a regional scale, respectively.

Plain Language Summary

Oxygen is fundamental to sustain life and to regulate carbon cycling in our Earth system. However, because of global warming, there is growing concern that oxygen in the ocean is declining, partly due to temperature increase and partly due to eutrophication that leads to excessive production of organic carbon which consumes oxygen during their degradation. In the worst case, the latter results in oxygen exhaustion, generating "dead zones" near/at the ocean seafloor. To mitigate this potential threat, it is important to understand the mechanisms that control oxygen consumption near and at the seafloor. To this end, our study provided a quantitative assessment of the driving factors for oxygen consumption across the sediment-water interface in a coastal sea. We found that animals living at the seafloor are of vital importance in controlling oxygen consumption in sediments. Therefore, it is important for us to protect benthic life and biodiversity, which in turn help to mitigate climate change through carbon preservation in seafloor.

Keywords

Benthic oxygen flux, Bioturbation, Early diagenesis, Biophysics, Benthic-pelagic coupling, Morphodynamics

1. Introduction

The ocean seafloor is the largest carbon reservoir within the surface Earth system, providing a valuable geochemical archive for deciphering variability in global biogeochemical cycling and climate (Ciais et al., 2013; Heinze et al., 2015). Quantification of biogeochemical cycling, especially carbon cycling at the ocean seafloor, is thus a key for understanding the fate of our future Earth (Falkowski et al., 2000; Le Quéré et al., 2018). Of vital importance in this context is the coastal shelf seafloor, which covers less than 10 % of the global ocean area (Muller-Karger et al., 2005) but has been estimated to receive ~50% of the pelagic primary production through sedimentation (Wollast, 1991) and releases regenerated nutrients such as nitrogen, phosphorus, and silica that supply ~80% of phytoplankton nutrient requirements (Middelburg & Soetaert, 2004). On the other hand, coastal shelf seas constitute the most dynamic part of the surface Earth where intense interactions between geosphere, ecosphere and anthroposphere take place. Ignoring or over simplifying such interactions leads to large uncertainties in calculating biogeochemical fluxes (e.g. Gattuso et al., 1998; Muller-Karger et al., 2005; Chen & Borges, 2009; Cloern et al., 2016; Griffiths et al., 2017), which may partly account for the imbalance of up-to-date estimates of global carbon budget (Le Quéré et al., 2018). Recent studies demonstrate a need to take into account spatial heterogeneity and biodiversity of the seafloor to better assess carbon processing and ecosystem functioning in the context of global biogeochemical cycles (Cardinale and Palmer, 2002; Lohrer et al., 2004; Belley and Snelgrove, 2016; Snelgrove et al., 2018). However, limited knowledge of the role of benthic organisms in modulating biogeochemical fluxes at the sediment-water interface impedes our ability to derive quantitative syntheses (Griffiths et al., 2017; Middelburg, 2018).

Benthic oxygen availability is fundamental to sustain aquatic life and to regulate many important biogeochemical processes including early diagenesis of organic carbon (Glud, 2008). A process-based understanding of how oxygen is transported into sediments and a quantification of its flux across the sediment-water interface is thus of utmost importance for evaluating benthic ecosystem functioning and biogeochemical cycling. Oxygen transport across the sediment-water interface evolves through the

advection and diffusion (Glud, 2008). Both transport mechanisms are controlled by not only hydrodynamic (porewater advection) and morphodynamic (bedform migration) processes but also by biophysical (bio-diffusion and bio-ventilation) and biogeochemical (degradation of OC) processes (Meile and Van Cappellen, 2005; Santos et al., 2012; Ahmerkamp et al., 2015). Benthic fauna contributes to both advective (through bio-ventilation) and diffusive (through bio-diffusion) transport, and significantly alters the efficiency of OC degradation by diffusing both OC and oxygen into subsurface sediments (Meile and Van Cappellen, 2005; Middelburg, 2018; Zhang et al., 2019). Therefore, benthic fauna may impose a major control on the benthic oxygen flux and biogeochemical cycling even on a regional to global scale (Griffiths et al., 2017; Snelgrove et al., 2018). However, a robust quantitative estimation of the impact of benthic fauna on the oxygen flux across the sediment-water interface is still lacking (Middelburg, 2018).

A mechanistic understanding of the interaction between benthic fauna and the associated environmental conditions must be derived before a quantitative synthesis can be made (Zhang and Wirtz, 2017). The abundance and community structure of benthic fauna greatly depend on the supply of particulate organic carbon (POC) to the seafloor (Pearson and Rosenberg, 1987; Dauwe et al., 1998; Herman et al., 1999; Campany à-Llovet et al., 2017). Bioturbation, referred to here as any kind of biological reworking of sediments including particle mixing and burrow ventilation (Meysman et al., 2006), has been found to vary by more than one order of magnitude even at the same site due to seasonal changes in food supply and in the metabolism of benthic organisms (Brown et al., 2004; Teal et al., 2008). The high variability of bioturbation clearly demands for its integration as a dynamic process in up-to-date ecosystem and diagenetic modelling (Queirós et al., 2015). Mechanistic approaches for quantifying bioturbation have been developed for more than three decades since the pioneering work by Berner (1980). Bioturbation is conventionally modelled as a diffusive mixing process (Berner, 1980; Boudreau, 1986a), and later on with inclusion of non-local transport (e.g., Boudreau, 1986b; Whearcroft et al., 1990; Soetaert et al., 1996a; Meysman et al., 2003; Holstein and Wirtz, 2009; Schiffers et al.,

2011; Aquino et al., 2017). However, although bearing the capacity of fitting individual tracer profiles, most existing bioturbation models are not designated for solving a dynamic benthic response to changing pelagic conditions, especially at a regional scale. Only a few ones explicitly relate macrobenthos and their bioturbation with settling POC (e.g. Butenschön et al., 2016; Zhang and Wirtz, 2017). Given the fact that POC supply is a major constraint for macrobenthos on one side, and macrobenthos is consumer as well as a major driver of POC transport in sediments on the other side, process-based modelling of the interaction between POC and macrobenthos and the consequent impact on benthic biogeochemical cycling deserves to be a focal point of research (Kelly-Gerreyn et al., 2014; Campany à-Llovet et al., 2017; Zhang and Wirtz, 2017).

In this study, we made a numerical modelling attempt to interpret the pattern of measured benthic oxygen fluxes in the south-eastern North Sea. Through a model reconstruction of the benthic dynamics in response to changing pelagic environmental conditions, we aim to provide a quantitative estimate of the importance of macrobenthos in controlling oxygen flux at the sediment-water interface at a regional scale. This goal necessitates the use of up-to-date 3-dimensional hydrodynamic-biogeochemical modelling, enabling to resolve the dynamic interactions between pelagic drivers and benthic biota, and subsequent impact on the early diagenesis of organic carbon, oxygen consumption and transport.

2. Material and methods

2.1. Study area

Our study area is the German Bight located in the south-eastern North Sea. This area is characterized by water depth up to 60 m, with its major part being shallower than 40 m (Figure 1a). Currents are predominantly driven by a combined action of wind and astronomical tides, and additionally modulated by baroclinity (Sündermann and Pohlmann, 2011) and river runoff (Becker et al., 1999). Semidiurnal tides M2 and S2 are the major tidal constituents. Energetic tidal currents with speed of up to ~2 m s^{-1} give rise to strong mixing and inhibit thermohaline stratification in a major part of the area (Schrum, 1997). A cyclonic residual circulation pattern exists in the German Bight due to an

interplay between different forces (wind-driven currents and tides) and topography (Nihoul, 1980). This circulation introduces a mixture of Atlantic water and river runoff (mainly Rhine, Meuse, IJsselmeer, Ems, Weser and Elbe) along the southern North Sea coast into the German Bight (van Beusekom et al., 1999) and favours deposition of fine-grained sediments (Figure 1b). Outcomes from the North Sea Observation and Assessment of Habitats (NOAH, 2013-2019) project (http://www.noah-project.de/habitatatlas/) indicate that the major part of the seafloor is dominated by sands (Figure 1c) with very limited organic content (Figure 1d). High sedimentation rates (up to 6 mm yr^{-1} on average, Dauwe et al., 1998) only occur on a few spatially confined mud deposits where silt and clay contents exceed 10% (Figure 1b). The distribution of fine-grained material on the seafloor is a joint effect of the residual circulation pattern and surface gravity waves (Stanev et al., 2009), both of which are strongly influenced by the seafloor topography especially that of the ancient Elbe river valley (Becker et al., 1999). Since fine-grained lithogenic sediments (silt and clay) tend to flocculate with organic matter during their transport (Maerz et al., 2016), the discrepancy between high mud content (> 10%) in several depocenters and high sedimentary TOC content (> 1%) confined in only one depocenter near the island Helgoland (Figure 1b & 1d) implies a strong benthic-pelagic coupling which significantly affects carbon storage and turnover in this productive area (Neumann et al., 2019).

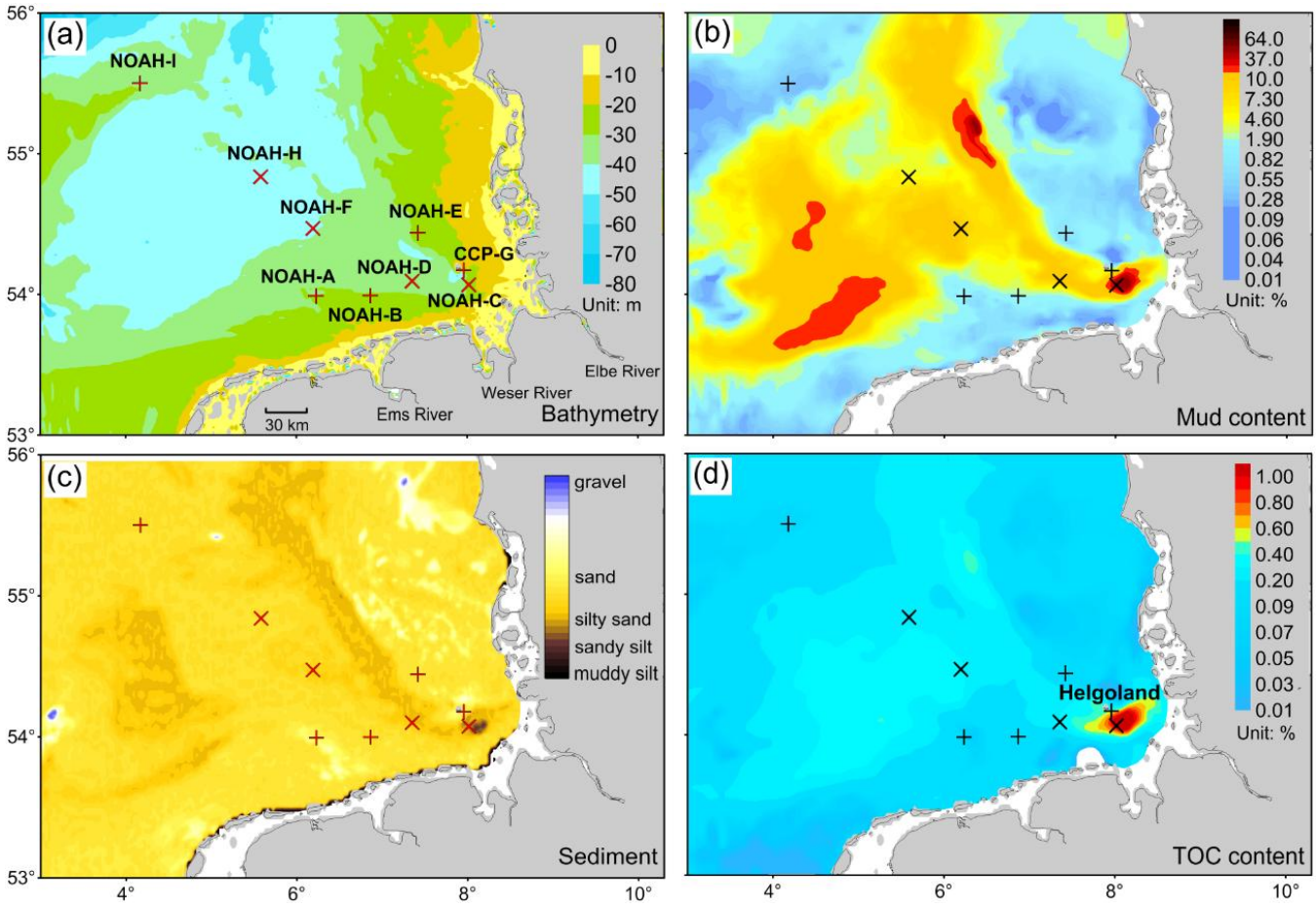

Figure 1. (a) Bathymetric map of the German Bight with marked sampling stations. (b) Mud content (%) in surface sediments plotted in logarithmic scale. (b) Classification of surface sediments according to the Folk's sand-silt-clay diagram. (d) TOC content (%) in surface sediments plotted in logarithmic scale. Note that the Wadden Sea area including the tidal channels between the barrier islands is not covered by the data. Sampling stations with permeable sediments are marked by ×, while stations with impermeable sediments are marked by +.

2.2. Field data

Measurement of benthic oxygen flux was done at 9 stations (Figure 1a) during cruises of the RV Heincke in 2012 – 2016 within the North Sea Observation and Assessment of Habitats (NOAH, 2013-2019) project (http://www.noah-project.de/habitatatlas/). Advective and diffusive fluxes were derived from in situ measurements using a benthic lander equipped with oxygen profilers (optodes) placed inside and above surface sediments and ex situ core incubation measurements, respectively.

2.2.1. In situ lander measurements

In situ measurements of advective oxygen flux induced by porewater flow were carried out in three months (March 2014, September 2014 and July 2015) at the stations with permeable sediments (Table 1). Technical details and results of the in situ measurements were presented by Ahmerkamp et al. (2017).

2.2.2. Ex situ incubation measurements

Ex situ core incubation measurements were done at all stations with the aim to derive the diffusive fluxes. The surface sediment was sampled with a Multicorer (Oktopus Kiel) equipped with acrylic (PMMA) core liners (10 cm inner diameter, 60 cm length). Typically, 3 to 4 intact sediment cores per station were selected for ex situ, whole-core, batch-type incubation. Cores with visible perturbations such as cracks, voids, or injured animals were rejected. The sediment cores were typically 15 - 30 cm in length. The incubations were closed with a gas-tight lids that were adjusted to a resulting supernatant height of 15 cm. The water column was constantly stirred by horizontal propellers (3 blades, 20 mm diameter) that were magnetically driven by external motors. The stirring intensity was adjusted so that it is low enough to prevent particle resuspension but on the other hand strong enough to ensure mixing of the supernatant and keep suspended particles from settling. It is noteworthy that porewater flow is minimized by this small stirring intensity so that the measured values represent the diffusive fluxes. Incubations were executed aboard the research vessel in a temperature-controlled lab at in situ temperature. Primary production was excluded by wrapping the cores in aluminium foil. During incubation, oxygen was monitored continuously with fiber-optical optodes (Presens). A two-point calibration was applied, employing air-saturated water (100 %) and oxygen-free water (0 %) that was prepared by addition of sodium sulphite (Na_2SO_3). The incubations were terminated when the oxygen saturation dropped below approximately 80 % saturation, which was typically after 12 to 24 h. Oxygen fluxes were calculated as concentration change over time by linear regression.

2.2.3. Complementary field data

In addition to measurement of benthic biogeochemical fluxes, sediment and macrobenthos samples were also collected from these stations by means of a Multicorer. Vertical distributions of TOC,

TOC/TN ratio and macrobenthos biomass in the upper-most 20 cm sediments were measured. Detailed processing procedures of these samples are described in Zhang et al. (2019). A list of substrate properties of the stations is provided in Table 1.

Table 1. *Substrate properties of the stations and sources*

Station	Median grain size d_{50} (μm)	Porosity ϕ (-)	Permeability k (m^2)	Mud (%)	TOC (%)	Bedform height l (cm)	Bedform length λ (cm)	Source
NOAH-A	390	0.40	1.1×10^{-10}	1.1	0.10	2.5	18	1&2
NOAH-B	210	0.42	3.2×10^{-12}	1.7	0.12	1.5	11	1&2
NOAH-E	249	0.41	4.5×10^{-11}	0.8	0.10	2.4	15	1&2
CCP-G	398	0.36	1.2×10^{-10}	3.0	0.30	2.7	22	1&2
NOAH-I	223	0.38	3.6×10^{-11}	0.4	0.08	1.5	11	1&2
NOAH-C*	35	0.53	0	52.0	1.10	-	-	1
NOAH-D*	102	0.45	0	10.0	0.31	-	-	1&2
NOAH-F*	128	0.50	0	10.0	0.33	-	-	1&2
NOAH-H*	155	0.46	0	6.0	0.27	-	-	1&2

Sources: (1) http://www.noah-project.de/habitatatlas/; (2) Ahmerkamp et al. (2017). Stations marked by * indicate impermeable sediments with $k < 10^{-12}$ m^2.

2.3. Numerical modelling of benthic oxygen flux

Oxygen input into sediment across the sediment-water interface consists of two terms, namely advection and diffusion, respectively. The flux Q_{O2} (μmol $m^{-2}h^{-1}$) is given by:

$$Q_{O2} = uC_0 + D\frac{(C_0 - C_1)}{\Delta z}, \qquad (1)$$

where u (m h^{-1}) is the interstitial seepage velocity normal to the seafloor surface, z is the depth (cm) with $z = 0$ at the sediment-water interface and positive downward, C_0 and C_1 (μmol m^{-3}) are the oxygen concentration at the sediment-water interface ($z = 0$ cm) and the centre of the first sediment cell ($z = 0.5$ cm in this study), respectively and D is the effective diffusivity (m^2 h^{-1}) calculated as the sum of molecular diffusivity (D_{mol}) and bioturbation diffusivity (D_b). The first term on the right hand side represents the advection term. The advection velocity equals zero ($u = 0$) in case of impermeable sediments. For permeable sediments, u equals to the sediment porosity (ϕ) times the porewater flow

velocity (Elliott and Brooks, 1997). A characteristic porewater flow velocity (u_p) is given by Ahmerkamp et al. (2015):

$$u_p = 2k\frac{U^2}{\phi\nu}\frac{\Delta p}{\lambda}, \qquad (2)$$

where k is the permeability, U is the bottom current velocity (m s^{-1}), ν (=10^{-6} m^2 s^{-1}) is the kinematic viscosity of water, Δp (=0.1) is a non-dimensional characteristic pressure difference and λ is the wave length of the bedform (ripples). A power-law decay of oxygen flux along an increasing dominance of bedform migration over porewater flow velocity is found by Ahmerkamp et al. (2017). To take into account this impact for permeable sediments, u is modified as:

$$u = \begin{cases} \phi u_p, & \text{if } c_{ph}/u_p < 1 \\ \phi u_p \left(\frac{c_{ph}}{u_p}\right)^{-1.66}, & \text{if } 6 \geq c_{ph}/u_p \geq 1, \\ 0.05\phi u_p, & \text{if } c_{ph}/u_p > 6 \end{cases} \qquad (3)$$

where c_{ph} is the bedform migration rate (m h^{-1}) that is dependent on the bed shear stress, bedform roughness and sediment grain size according to Ahmerkamp et al. (2015).

Molecular diffusivity is determined by sediment porosity (ϕ), tortuosity (τ) and ambient temperature (T in °C), and calculated by (Soetaert et al., 1996b):

$$D_{mol} = (D_0 + D^* T)\frac{1}{\tau}, \qquad (4)$$

where D_0 is the molecular diffusion coefficient of oxygen at 0 °C and D^* is the diffusion coefficient for linear temperature dependence of oxygen. Tortuosity (τ) is calculated from the sediment porosity as

$\tau = F\phi$ with $F = \phi^{-m}$, where m=2 is for marine sands or muds with $\phi \le 0.7$ and m=3 for high-porosity muds with $\phi > 0.7$ (Ullman and Aller, 1982).

Bioturbation diffusivity (D_b) is calculated by a mechanistic model, namely the TOC-MAcrobenthos Interaction Model (TOCMAIM), which has been calibrated and validated by field data from the North Sea (Zhang & Wirtz, 2017; Zhang et al., 2019). Given a boundary input of OC at the sediment-water interface, TOCMAIM solves the mass balance equation of OC in surface sediments by including the impacts of sedimentation (through advection), first-order degradation, macrobenthic uptake and bioturbation (through diffusion). Bioturbation diffusivity D_b for solutes in this study is assumed to be 10 times the bioturbation diffusivity for solids. D_b scales with the local macrobenthos biomass B through a power law and inversely proportional to local food resource (OC):

$$D_b = 10\beta B^b \left(\sum_{i=1}^{3} a_i C_{org,i}\right)^{-1}, \qquad (5)$$

where β, b are empirical parameters linking body-size and abundance to biomass. Biomass of macrobenthos (B) is estimated in TOCMAIM based on local food resource (i.e. OC content) and costs for respiration and mortality (Zhang & Wirtz, 2017). Organic carbon is divided into three pools ($C_{org,i}$, i=1,2,3) depending on the degradability, namely labile (i.e., of high quality nutrient), semi-labile (i.e., of intermediate quality nutrient) and refractory (i.e., of low quality nutrient). a_i ($i = 1, 2, 3$) are coefficients representing the yield of the POC pool i in terms of gaining macrobenthos biomass, with higher quality OC gaining biomass more efficiently, as expressed by $a_1 > a_2 > a_3$. The above formulation explicitly links the bioturbation diffusivity with (1) the body-size and abundance of macrobenthos (through scaling with biomass), and (2) the local food resource which determines the intensity of vertical movements of macrobenthos to derive enough energy and nutrition for metabolism and growth. A detailed justification of Equation (5) is provided in Zhang & Wirtz (2017).

It can be seen from Equation (1) that the oxygen flux depends on not only the diffusivity but also on the vertical gradient of oxygen concentration across the sediment-water interface, i.e. $(C_0 - C_1)/\Delta z$. In this study, pelagic environmental variables such as current velocity, bottom shear stress, temperature, POC concentration and oxygen concentration at the sediment-water interface $z = 0$ cm (i.e. C_0) are provided by a 3-D hydrodynamic-biogeochemical model ECOSMO II (Schrum et al., 2006a, b; Daewel & Schrum, 2013), while POC burial, transport and degradation in sediments including the interaction with macrobenthos are simulated by the coupled model TOCMAIM (Zhang et al., 2019). A new feature of TOCMAIM introduced in this study is an inclusion of oxygen consumption in sediments by solving the mass balance equation assuming that oxygen is exclusively consumed by POC degradation:

$$\frac{\partial C}{\partial t} = -\frac{\partial wC}{\partial z} + \frac{\partial}{\partial z}(D\frac{\partial C}{\partial z}) + S - \frac{(1-\phi)}{\phi}\varepsilon\sum_{i=1}^{3} R_i C_{org,i}\ , \qquad (6)$$

where C denotes oxygen concentration (μmol m^{-3}), w is the advection (sedimentation) rate (m h^{-1}), S is the source term being equal to $uC_0/\Delta z$ for the first (upper-most) sediment cell and zero for the rest cells, R_i is the depth-dependent first-order degradation rate constant of POC pool i ($C_{org,i}$), and is calculated by $R_i(z) = e^{-0.3z}R_i(0)$, where $R_1(0) = 2.3\times10^{-3}$ h^{-1}, $R_2(0) = 2.3\times10^{-4}$ h^{-1} and $R_3(0) = 2.3\times10^{-6}$ h^{-1}, and ε is a constant representing the ratio of oxygen demand to carbon degradation. A list of model parameters is given in Table 2, with further details of TOCMAIM and its coupling to ECOSMO II provided in Zhang et al. (2019).

Table 2. *Model parameters and sources*

Parameter	Unit	Value	Source
D_0	$cm^2\ h^{-1}$	0.04	1
D^*	$cm^2\ h^{-1}\ °C^{-1}$	1.6×10^{-3}	1
β	-	0.22	2
b	-	1.33	2

a_1	h^{-1}	0.03	2
a_2	h^{-1}	0.01	2
a_3	h^{-1}	1.7×10^{-3}	2
ε	-	1.45	3

Sources: (1) Hülse et al. (2018); (2) Zhang and Wirtz (2017); (3) Hedges et al. (2002).

It can been seen from Table 1 that sediment permeability differs markedly between stations. In our study, a tested empirical relationship associating permeability with sediment grain size proposed by Neumann et al. (2017) was adopted to provide sediment permeability map for the entire study area with 1.852 ×1.852 km grid resolution. The derived map (https://www.noah-project.de/habitatatlas/index.php.en) shows that 25% of the seabed in the study area is covered by impermeable sediments ($k < 10^{-12}$ m^2) and the rest by permeable sands. For predicting the bedform parameters (l and λ), we applied the widely-used formulation from Soulsby et al. (2012) validated for the southern North Sea by Krämer and Winter (2016). By feeding the permeability map and bedform predictor into the 3D hydrodynamic-biogeochemical model, the benthic oxygen flux for the entire German Bight (Figure 1) from 2012 to 2016 was calculated.

3. Results

3.1. Observed Benthic Oxygen Flux

Advective fluxes across the sediment-water interface at permeable sediments measured in situ by lander are characterized by relatively small variations in July and enhanced variations in March and September (Figure 2a). The exact values range between 330 and 1420 μmol m^{-2} h^{-1} among the sampling stations. It is difficult to judge whether a seasonal pattern exists in the advective flux due to limited number of observations.

The median standard error of diffusive oxygen flux single incubations was 0.12, and had little variation. The relative error of the average fluxes at a given site was in the range of 0.1 – 0.5 during winter and early summer, while the relative variation of flux increased considerably to the range of 0.2 –

1.4 during summer. The observed fluxes of oxygen at the different study sites had similar seasonal patterns (Figure 2b). Fluxes were low during winter (January – March) with a magnitude of 250 µmol m^{-2} h^{-1}. Starting in spring (end of March), fluxes generally increased substantially and peak at the summer – autumn transition (September). The maximum fluxes observed in late summer were as high as 2000 µmol m^{-2} h^{-1}. After the late summer, benthic fluxes decreased rapidly and remained low during autumn and winter. However, sampling density was low during November and December.

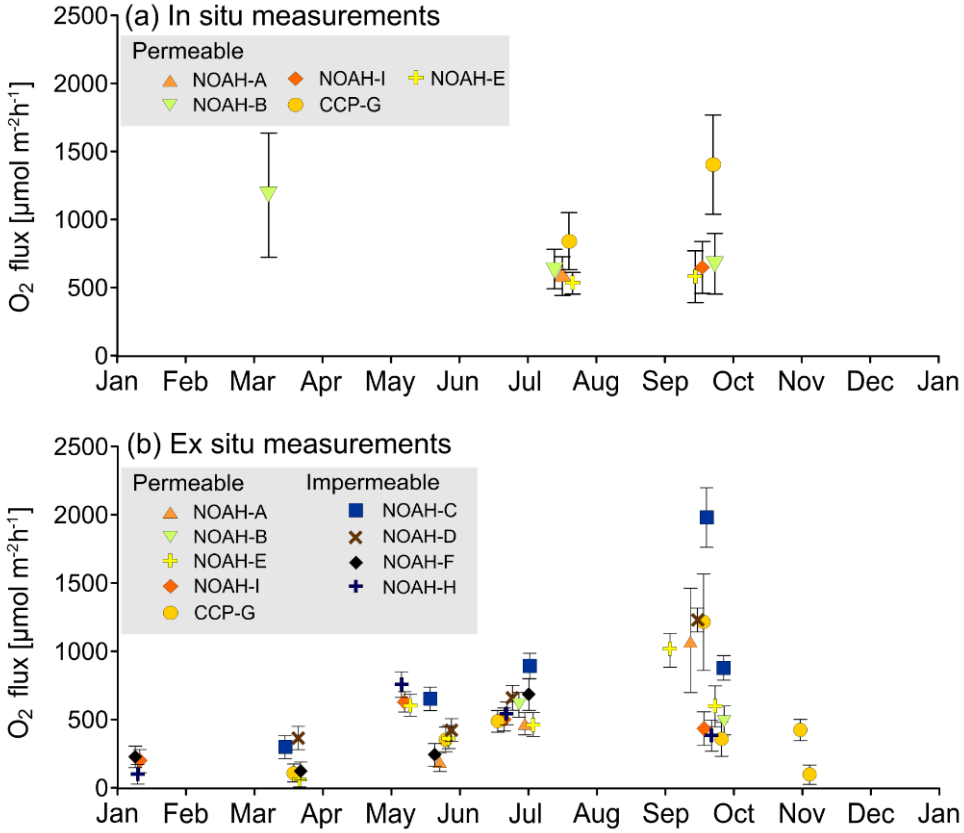

Figure 2. Temporal variation of measured oxygen flux (mean ± standard deviation) across the sediment-water interface at the sampling stations using (a) in situ lander (Ahmerkamp et al., 2017), and (b) ex situ core incubation chambers.

3.2. Simulation Results

3.2.1. Comparison Between Model Results and Field Data

A comparison between the measured and simulated oxygen flux across the sediment-water interface at the sampling stations demonstrates a general satisfactory model performance (Pearson's r = 0.67) in capturing both spatial and temporal variations of benthic oxygen flux (Figure 3a), though the

model tends to overestimate oxygen flux in case of large values (> 800 μmol m^{-2} h^{-1}). Detailed simulation results and comparison with observation at each sampling station are provided in the Supplemental Information.

A critical state variable that is relevant to benthic oxygen dynamics and can be directly compared to field data is macrobenthos biomass. An agreement between the measured and simulated macrobenthos biomass (Figure 3b) has been already demonstrated in Zhang et al. (2019). In contrast to the overestimation of oxygen flux, macrobenthos biomass is slightly underestimated in the model result for values larger than 8 g C m^{-2}. It is worth noting that macrobenthos biomass ranges between 1 and 9 g C m^{-2} at the sampling stations, except for the station NOAH-C (>10 g C m^{-2}) which is located at the mud depocenter adjacent to the Helgoland island, where the highest content of both mud and TOC in the study area is located (Figure 1, Table 1).

The good model performance allows for using the simulation results to derive insights into the relationship between pelagic drivers and benthic response in terms of oxygen dynamics. Despite of a large variability in observed values of oxygen flux among the stations, the seasonality of oxygen flux at most sampling stations shares a large degree of similarity. Accordingly, our simulation results at all stations are analyzed as ensemble in the following, so that a common pattern of benthic-pelagic coupling in response to seasonality of driving forcing can be inferred.

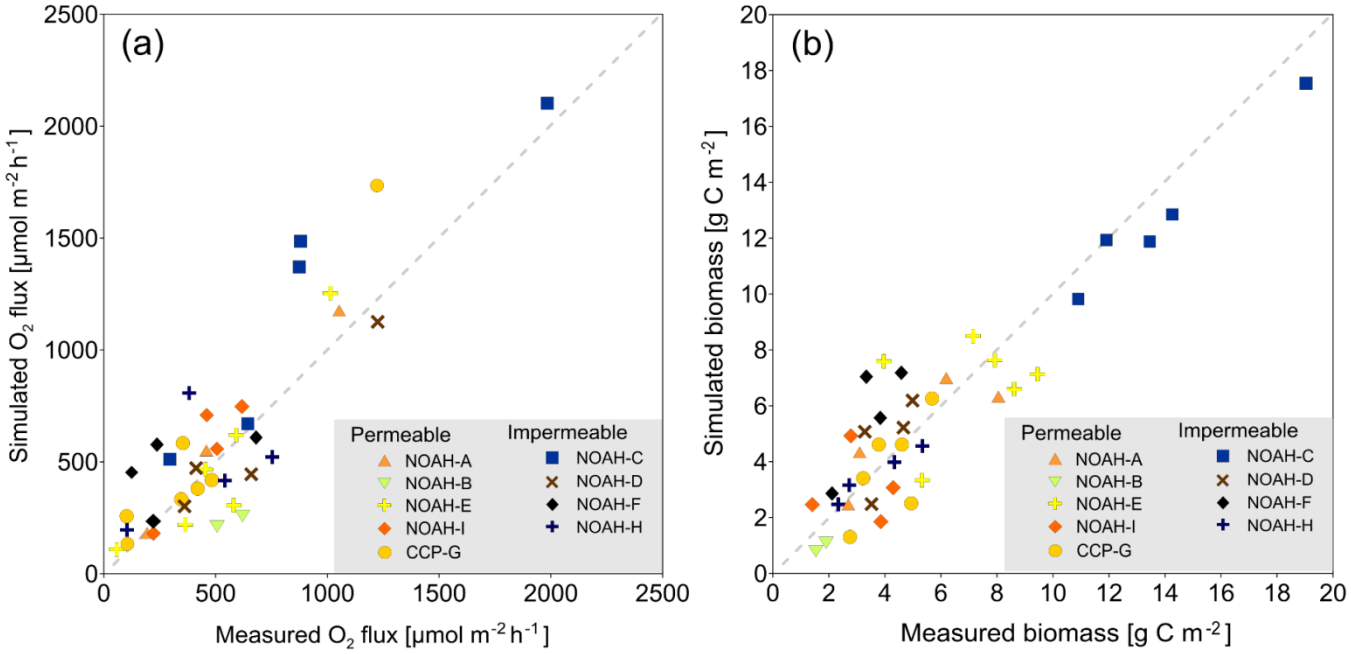

Figure 3. Comparison between model result and field data of (a) oxygen flux across the sediment-water interface, and (b) macrobenthos biomass (in ash free dry weight) at the sampling stations. Note that in (a) the simulated advective flux induced by porewater flow is deducted from the model result for consistency with the measurement using ex situ incubation chambers.

3.2.2. POC at Sampling Stations - Pelagic Drivers

Simulated concentration of phytoplankton biomass (measured in POC) at the nine sampling sites, which reflects primary productivity in the study area, indicate that despite of large difference in the magnitude, an annual cycle with significant seasonality exists at each station (Figure 4a). The time series of simulated phytoplankton biomass at all stations in all years (2012 – 2016) are characterized by a low level (90th percentile < 20 mg C m^{-3}) in the cold season between early November and mid-February, a drastic increase since late February till mid-March indicating an early spring bloom (median = 80 mg C m^{-3} at the stations), a subsequent mild decline and then a second and even stronger bloom (median = 120 mg C m^{-3}) in late spring, followed by a sharp decline (median = 25 mg C m^{-3}) in late May and then several pulses of mildly enhanced production (median between 45 and 60 mg C m^{-3}) until mid-to-late September (Figure 4a).

Although POC originating from fresh plankton detritus is relatively abundant in bottom water since the early spring bloom, the strength of bottom current and turbulence in the benthic boundary layer

control whether the POC can settle on the seafloor. Simulations indicate that bottom currents are energetic between early October and late March (in the following year) with median bottom shear stress exceeding the threshold of sediment mobilization (0.05 N m^{-2}). Bottom hydrodynamic regime becomes favorable for POC deposition from April to September, with calmest condition in July and August when median bottom shear stress is less than 0.025 N m^{-2}. A further decrease of shear stress below 0.01 N m^{-1} allows settling down of POC on the seafloor, which is mostly confined between April and September (Figure 4b).

The simulated bottom water temperature, which is validated by observation (Figure 4c), indicates a minimum (median = 4.3 °C) in early March and a maximum (median = 18 °C) in early September among the stations in 2012 – 2016. Variation in bottom temperature between October and March is confined to a narrow band (±4 °C between the 90th and 10th percentile), while a larger variation (±6-7 °C between the 90th and 10th percentile) occurs in summer from June to August. Simulated bottom water oxygen concentration (Figure 4d) shows a negative correlation (Pearson's r = -0.91) with the temperature. Its median value ranges between 4.4 and 7.3 ml L^{-1} among different seasons at the sampling stations.

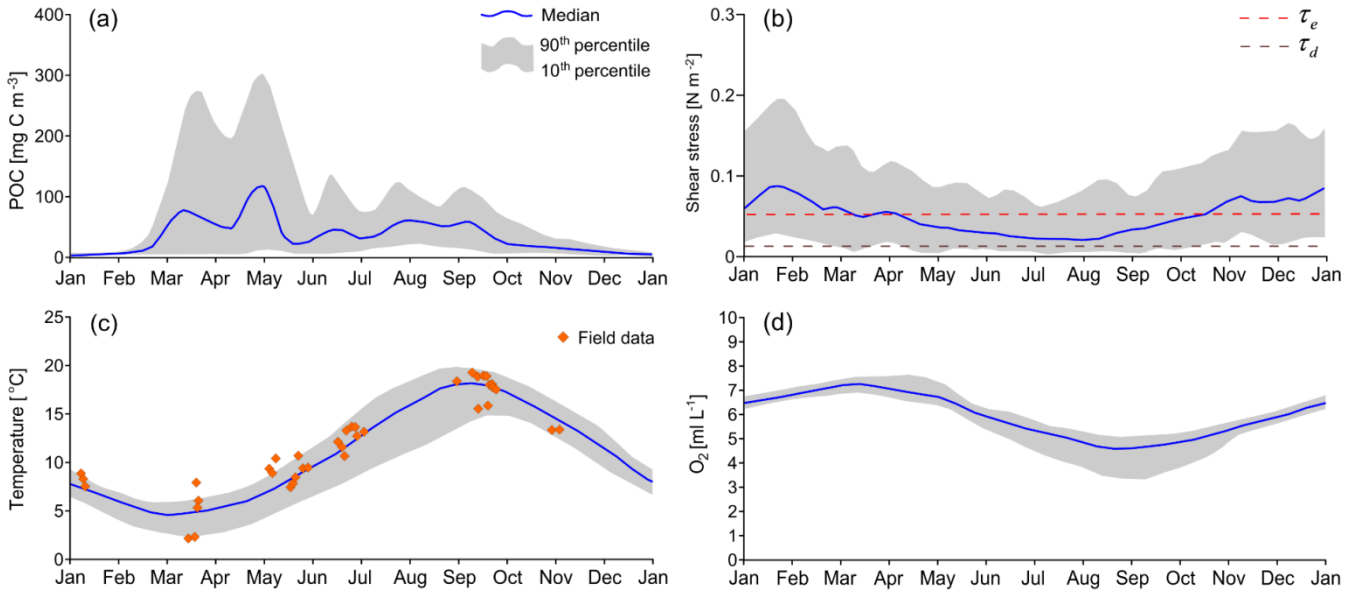

Figure 4. Simulated temporal (2012-2016) variation of (a) bottom water POC concentration, (b) daily-mean bottom shear stress, (c) bottom water temperature, and (d) bottom water oxygen concentration at the sampling stations. Values between the 10th and the 90th percentiles are indicated by the grey area, within which the median is marked by the solid curve. The thresholds for calculating sediment mobilization (τ_e = 0.05 N m^{-2}) and deposition of organic detritus (τ_d = 0.01 N m^{-2}) are indicated in (b) by the dashed lines. Field measurements of bottom water temperature at these stations are included in (c). Note that the large range between the 10th and the 90th percentiles in plots (a) and (b) is attributed mainly to spatial variation among the stations.

3.2.3. Benthic Response at Sampling Stations

The seasonality of shear stress induces a distinct seasonal pattern of POC fluxes across the sediment-water interface with net erosion in the cold season and net deposition in the warm season. These two regimes alternate in early March and early October (Figure 5a).

The settled POC serves as the main food resource for macrobenthos. The simulated macrobenthos biomass shows a rapid response to the POC input and output fluxes (Figure 5b). Macrobenthos biomass is at its minimum (median = 60% of the annual mean) in late February/early March due to shortage in food (POC), and starts to increase in response to POC input, reaching its maximum (median = 134% of the annual mean) in late August. This seasonal pattern is paralleled by the simulated bioturbation diffusivity D_b (Figure 5c). Minimum and maximum bioturbation rates were calculated for February (median = 70% of the annual mean) and August (median = 130% of the annual mean), respectively.

Bioturbation comes with two contrasting effects on POC preservation in sediments. On the one side, macrobenthos mixes down oxygen into sediments and facilitates degradation of POC. On the other side, bioturbation induces transport of labile POC into deeper horizons of sediment where degradation efficiency is slowed down due to oxygen deficiency. Our simulations show that there is a net positive impact of bioturbation on preservation of POC in sediments (Figure 5d), indicating that the amount of POC transported into sediments by bioturbation exceeds the amount of remineralized POC in surface sediments, making subsurface sediments a net sink of POC. The simulated temporal variation of labile and semi-labile POC (originated from fresh plankton detritus) in the uppermost 10 cm-surface sediments is characterized by one-month delay in reaching its maximum (mid-September) and an accelerated decline afterwards, indicating a slightly different pattern compared to the variation of macrobenthos biomass. Further, the efficiency of labile and semi-labile POC preservation in the cold season (from January to March) varies remarkably among the stations, with a median = 55% of the annual mean.

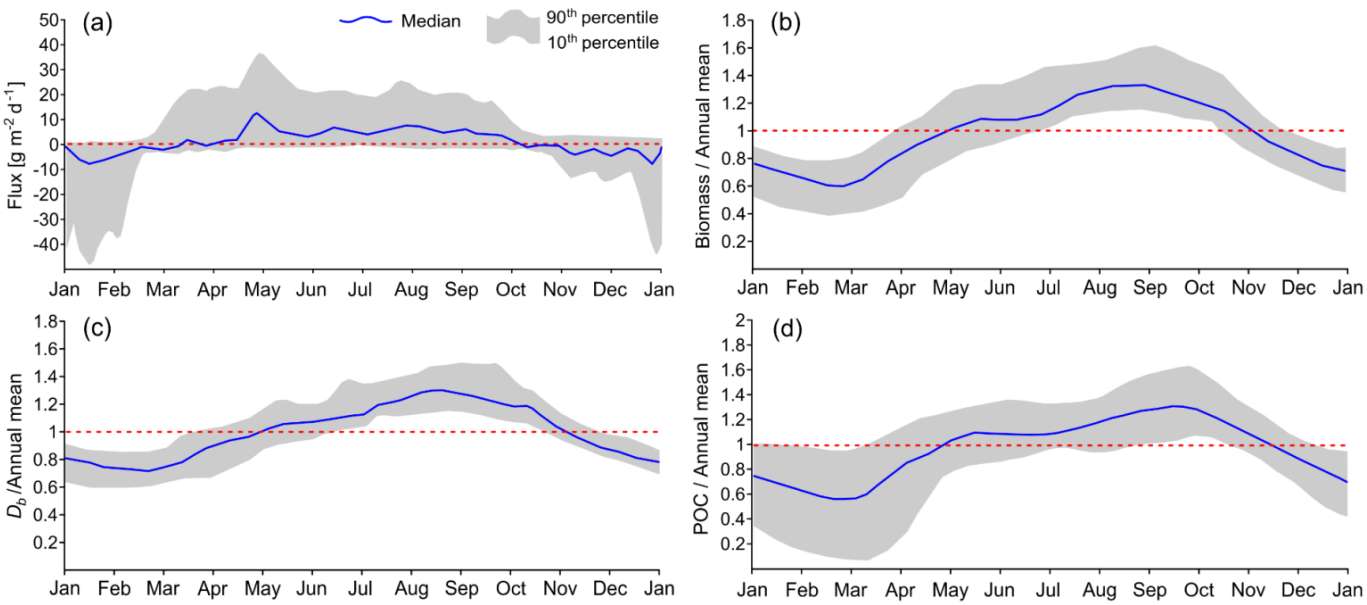

Figure 5. Simulated temporal (2012-2016) variation of (a) daily POC flux across the sediment-water interface with positive/negative value indicating deposition/erosion, (b) biomass of macrobenthos divided by the respective annual mean, and (c) bioturbation diffusivity D_b divided by the respective annual mean, and (d) labile and semi-labile POC content of surface sediments (uppermost 10 cm) divided by the respective annual mean at the sampling stations.

Oxygen fluxes across the sediment-water interface markedly change as soon as POC settles on the seafloor due to OC remineralization being influenced by both temperature and bioturbation. Despite of large difference in the magnitude of values among the stations (as shown by a large range between the 10th and the 90th percentile in Figure 6), a similar annual cycle is seen at most sampling stations (see Supplemental Information). Simulations (Figure 6a) show that the total oxygen flux transported into sediments remains on a relatively low level from December to March (in the following year) at most stations, characterized by a median value < 800 $\mu mol\ m^{-2}\ h^{-1}$. The flux increases from March onward, exhibits a mild peak in early May at some stations in some years (especially in 2013, see Supplemental Information), and then rises again with an accelerated rate from July till reaching its maximum in late August/early September (median = 1450 $\mu mol\ m^{-2}\ h^{-1}$). The flux decreases from mid-September to November, in accordance with the observation (Figure 2). A decomposition of processes contributing to the total oxygen flux reveals opposite temporal variations between the advection (Figure 6b) and the diffusion (Figure 6c, d). The advective flux contributes to a major part of the total flux in permeable sediments from mid-October to mid-June (in the following year) with the median exceeding 50% of the total flux (Figure 7a), and its 90th percentile may even reach to 90% at some stations. However, both the advective flux and its relative contribution to the total flux drop quickly from June onward with its median value accounting for less than 40% of the total flux in August and early-September. By contrast, diffusive flux remains relatively low in the cold season and peaks in the warm season (Figure 6c, d). Despite of a similar variation pattern, molecular diffusion and bio-diffusion differ significantly in magnitude. Molecular diffusion accounts only for a minor portion (median < 9%) of the total flux (Figure 7b), while bio-diffusion contributes to a significant portion (15% in cold seasons and 62% in warm seasons as median) of the total flux in permeable sediments (Figure 7c) and more than 85% in impermeable sediments (Figure 7d).

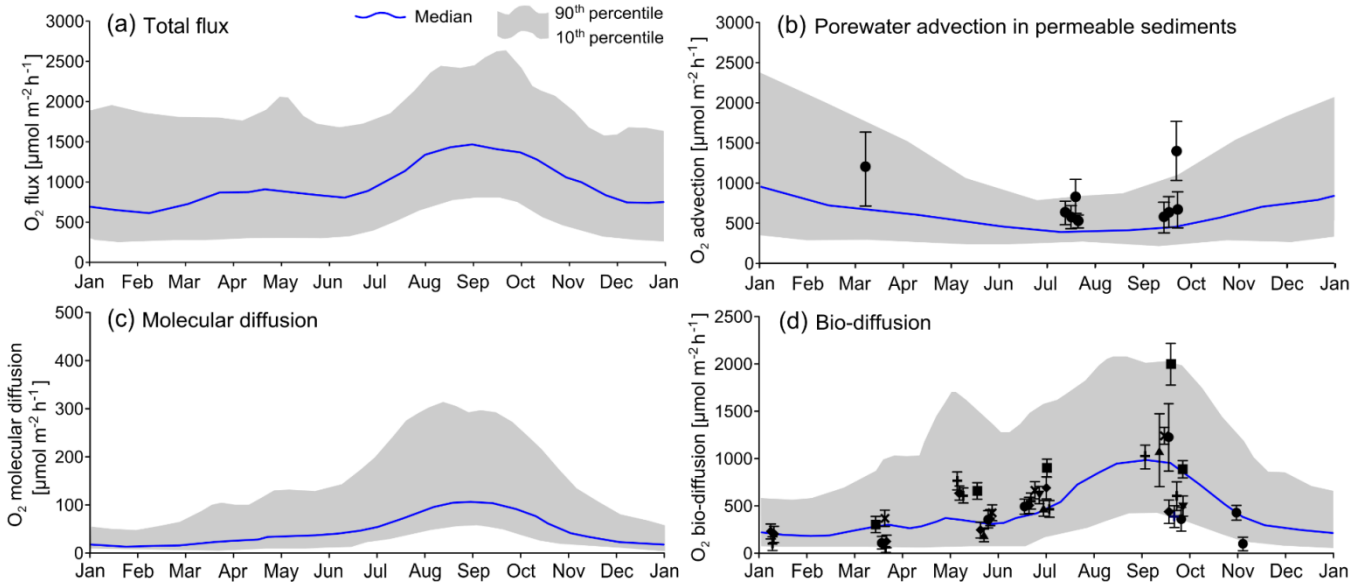

Figure 6. Simulated temporal (2012-2016) variation of (a) total oxygen flux across the sediment-water interface, (b) advective flux induced by porewater flow, (c) molecular diffusive flux, and (d) bio-diffusive flux at the sampling stations. Note that the large range between the 10th and the 90th percentiles in the plots is attributed mainly to spatial variation among the stations. Measurements of advective and diffusive oxygen fluxes are included in (b) and (d), respectively.

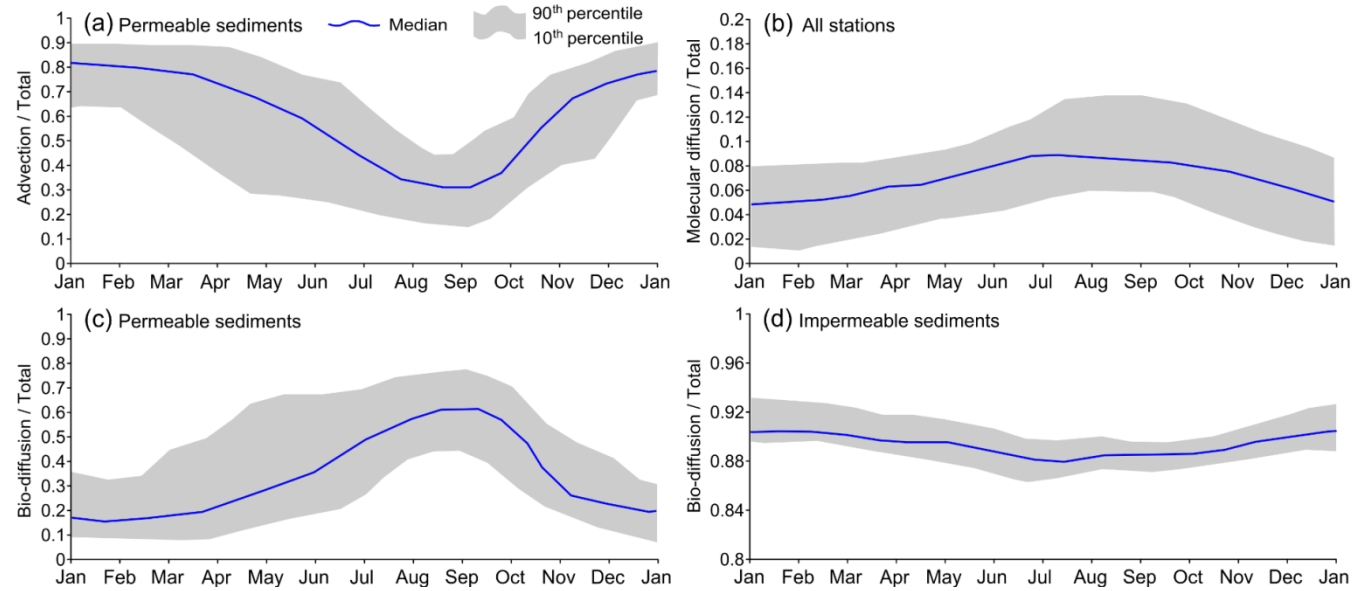

Figure 7. Simulated temporal (2012-2016) variation of the relative contribution of (a) advection to the total flux of oxygen at permeable sampling stations, (b) molecular diffusion to the total flux of oxygen at all sampling stations, (c) bio-diffusion to the total flux of oxygen at permeable sampling stations, and (d) bio-diffusion to the total flux of oxygen at impermeable sampling stations. Note that the large range between the 10th and the 90th percentiles in the plots is attributed mainly to spatial variation among the stations.

3.2.4. Benthic Oxygen Flux at Regional Scale

Simulation results of benthic oxygen flux at a regional scale (German Bight) exhibit a complex distribution characterized by patches of hotspots (Figure 8a). A decomposition into advective and diffusive components helps to quantify their respective contribution to the spatial variability and to unravel driving mechanisms behind that.

Results show that the contribution of molecular diffusion is minor, with a mean annual value below 200 $\mu mol\ m^{-2}\ h^{-1}$ in a major part of the area and accounting for less than 10% of the total flux. This result is consistent with the result at the sampling stations. It is worth to note that the molecular diffusion is in general higher in offshore area (water depth > 40 m) than in nearshore area, except for the part around the Helgoland island and off the Elbe estuary (Figure 8b).

In contrast to the spatial pattern of molecular diffusive flux, the advective flux is higher in nearshore area (water depth < 40 m) with a mean annual value in general above 300 $\mu mol\ m^{-2}\ h^{-1}$, even reaching to more than 1000 $\mu mol\ m^{-2}\ h^{-1}$ in some of the hotspots (Figure 8c). We identified a clear link between these hotspots and sediment grain size, and found that the 250 μm (d_{50}) median grain size contour can be used as a geographic indicator for the extent of hotspots for advective flux (Figure 8c). Two sampling stations (NOAH-A and CCP-G) are located within these hotspots as evidenced by field observations showing higher values at these two sites (see Supplemental Information). A significant part (~25%) of the study area, e.g. the ancient Elbe river valley and the mud depocenter off Helgoland, is covered by impermeable sediment where advective oxygen flux is zero.

The spatial distribution of bio-diffusive flux shows a high correlation with macrobenthos biomass. Hopspots of bio-diffusive flux (> 800 $\mu mol\ m^{-2}\ h^{-1}$) are normally confined in areas where macrobenthos biomass exceeds 5 g C m^{-2} in ash free dry weight (Figure 8d). These areas include both muddy and sandy seafloors. A comparison with our previously published results for distrbution of dominant benthic

community structure (Figure 7 in Zhang et al., 2019) indicates that in the muddy hotspots the diffusive flux is mainly contributed by deposit feeders while in the sandy hotspots it is mainly caused by surface feeding animals including suspension and filter feeders.

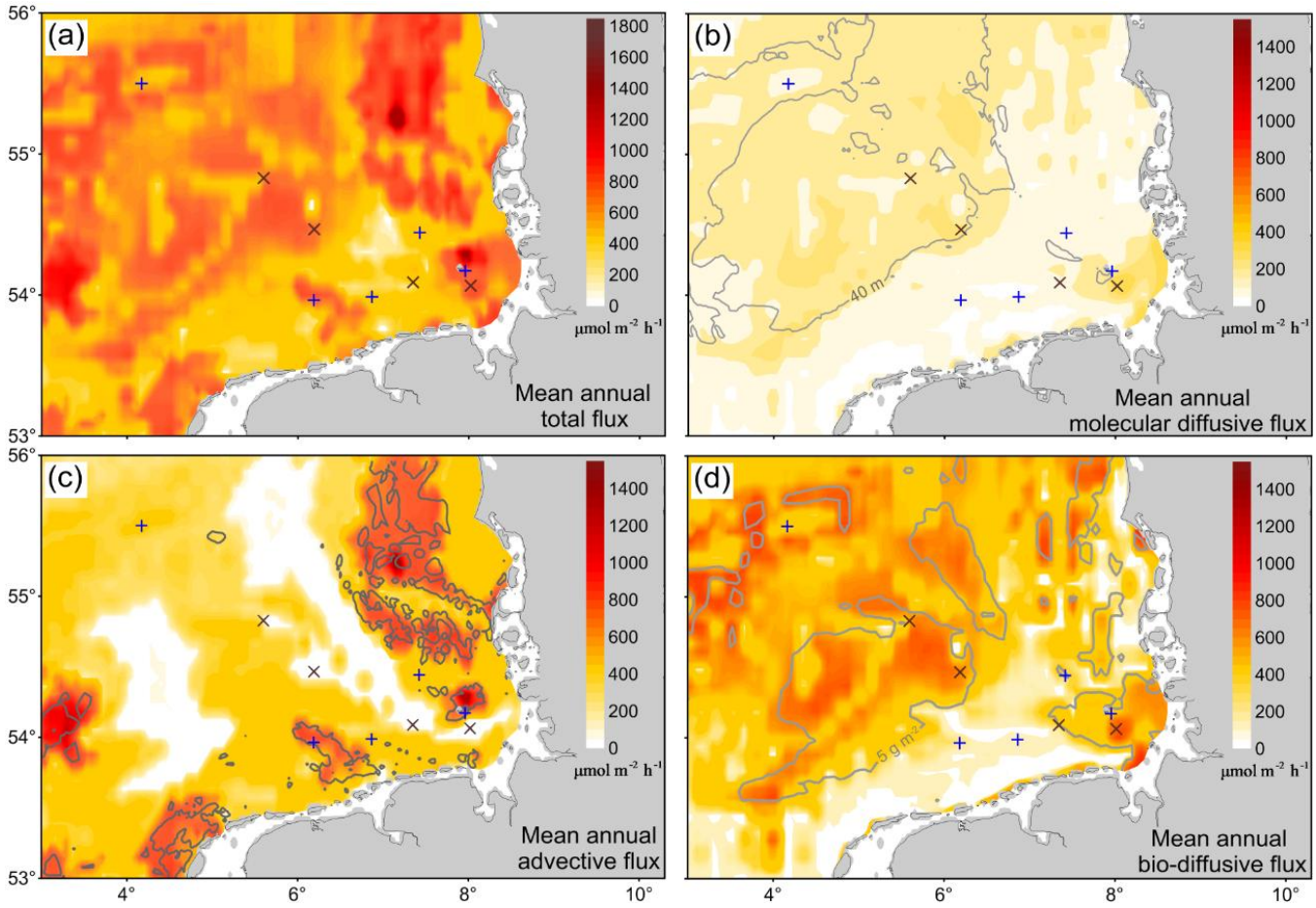

Figure 8. Simulated mean annual total oxygen flux (2012-2016) across the sediment-water interface (a) and its components (b, c, d) in the German Bight with marked sampling stations. Note that the Wadden Sea area including the tidal channels between the barrier islands is not covered by the data. The 40 m water depth contour is indicated in (b). The 250 µm (d_{50}) median grain size contour is indicated in (c) and the 5 g C m^{-2} macrobenthos biomass contour is indicated in (d).

To aid further interpretation, results for the entire study area are averaged spatially according to the sediment type (i.e. permeable and impermeable). Distinct patterns are shown between the two sediment types (Figure 9a, b). Similar to the results at the sampling stations, benthic oxygen flux in permeable sediments is predominantly controlled by porewater advection in the cold season and significantly modulated by bio-diffusion in the warm season (Figure 9c). At an annual scale, advection and bio-

diffusion contribute to 52 ± **7** % and 45 ± 9 % of the total oxygen flux in permeable sediments that cover ~75% of the study area. A combination of the opposite seasonal varying patterns of advection and diffusion results in a mild variation (median between 1200 and 1600 μmol m^{-2} h^{-1}) of the total oxygen flux in permeable sediments throughout the year at a regional scale (Figure 9a). By contrast, a much stronger seasonal variation pattern (median between 700 and 1700 μmol m^{-2} h^{-1}) dominated by bio-diffusion is shown in impermeable sediments with less annual variability at a regional scale (Figure 9b, d). At an annual scale, bio-diffusion contributes to 87 ± 4 % of the total oxygen flux in impermeable sediments of the study area. The range of our results is generally supported by various field measurements from the southern North Sea compiled by Provoost et al. (2013) and Ahmerkamp et al. (2017) showing that the benthic oxygen flux varies widely between 40 and 2500 μmol m^{-2} h^{-1} (i.e. 1-60 mmol m^{-2} d^{-1}) at individual stations with most values between 400 and 1700 μmol m^{-2} h^{-1} (i.e. 10-40 mmol m^{-2} d^{-1}).

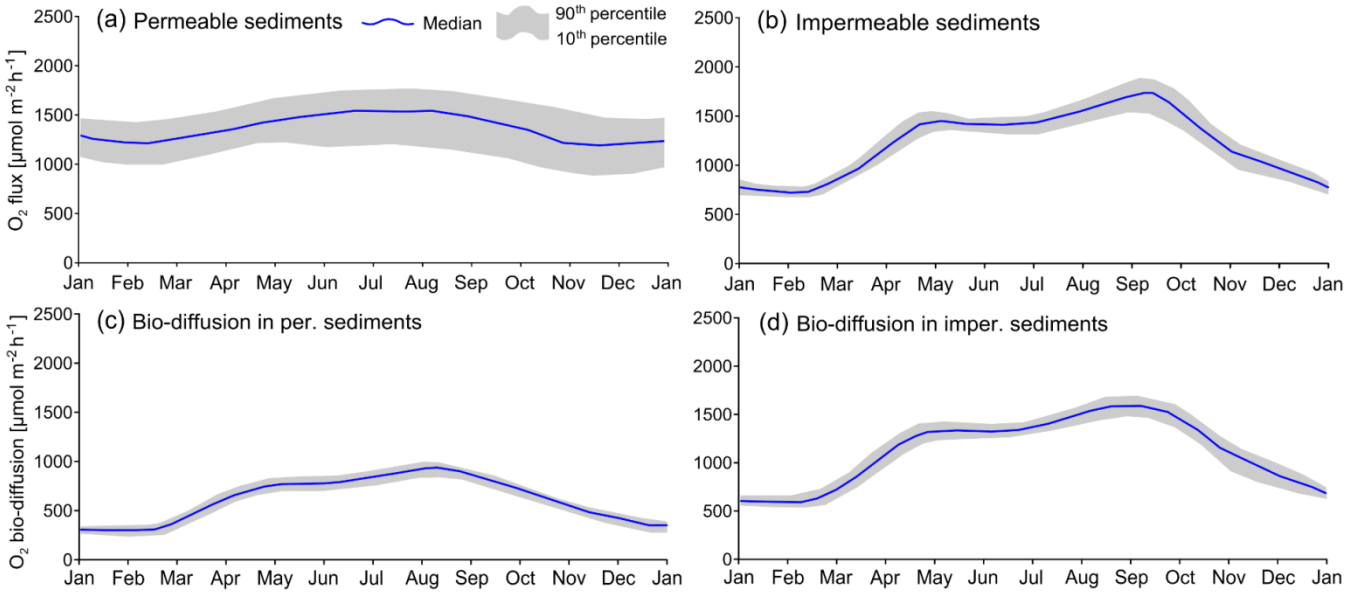

Figure 9. Simulated temporal (2012-2016) variation of spatially-averaged total oxygen flux across the sediment-water interface in (a) permeable sediments and (b) impermeable sediments, and the component induced by bio-diffusion in (c) permeable sediments and (d) impermeable sediments. Note that the 10th and the 90th percentiles and the median value refer to the annual variation.

3.2.5. Quantitative importance of bioturbation

It can be seen from Equation (1) and (6) that bioturbation not only directly diffuses oxygen across the sediment-water interface, but also indirectly influences the oxygen flux through a transport and mixing of the electron donor, i.e. POC, thereby changing the consumption rate of oxygen and the consequent vertical gradient of oxygen. To further assess the role of bioturbation, a new simulation with exclusion of bioturbation (termed No_D_b hereafter) was done, and results are compared with those including bioturbation (termed reference result hereafter).

Simulation results of No_D_b differ significantly from both the observation and the reference result in not only the magnitude of the total flux but also the seasonal variation pattern (Figure 10a, b). Results of No_D_b show that in permeable sediments, the total oxygen flux is predominantly controlled by porewater advection that takes up more than 70% during most of the year. The diffusive oxygen flux constantly ranges below 200 $\mu mol\ m^{-2}\ h^{-1}$ in permeable sediments, which is much lower than the observed values (Figure 2). In contrast to the advection-dominated permeable sediments, oxygen flux is determined solely by molecular diffusion in impermeable sediments and exhibits a similar variation pattern with observation and the reference result, but with a much smaller magnitude (Figure 10b). Its median value in cold and warm seasons account for only 25% and 15% of the median of the observed values in the respective periods. Such huge discrepancy between the simulation results of No_D_b and observation demonstrates that a major portion of the observed oxygen flux is attributed to biotic factors (bio-diffusion/bio-ventilation) instead of abiotic factors (molecular diffusion).

The indirect impact of bioturbation on oxygen consumption through a transport and mixing of POC is reflected by comparison of modelled molecular diffusion between No_D_b and the reference result. The comparison reveals a two-sided effect of bioturbation on the molecular diffusive flux (Figure 10c). In stations characterized by energetic bottom currents and low POC depositional rate (e.g. CCP-G), bioturbation effectively preserves POC in sediments and increases benthic oxygen consumption fuelled

by the transport of electron acceptors via porewater-advection compared to that in No_D_b, in which case POC is simply deposited at the surface and subsequently resuspended and carried away by currents. Bioturbation results in an enhanced molecular diffusive flux in the reference result compared to that of No_D_b. Such enhancement is reflected in the median value of the ratio of the simulated molecular diffusive flux in No_D_b to the reference result, which is below one during most time of the year (Figure 10c). On the other hand, when bottom currents are persistently weak and POC depositional rates are high (e.g. NOAH-C), bioturbation transports a significant portion of POC into deeper sediments where oxygen is deficient, thereby reducing oxygen consumption in the upper-most sediment layer. The resulting molecular diffusive flux across the interface is greatly reduced compared to that in No_D_b. This is reflected in the 90th percentile of the ratio of the simulated molecular diffusive flux in No_D_b to the reference result, which exceeds 1.4 all year round (Figure 10c). It is worth to note that although bioturbation results in a reduction of oxygen consumption in the upper-most sediment layer, it increases oxygen consumption beneath this layer by mixing down oxygen into deeper sediments, resulting in a flux much higher than that induced by molecular diffusion alone (Figure 8d).

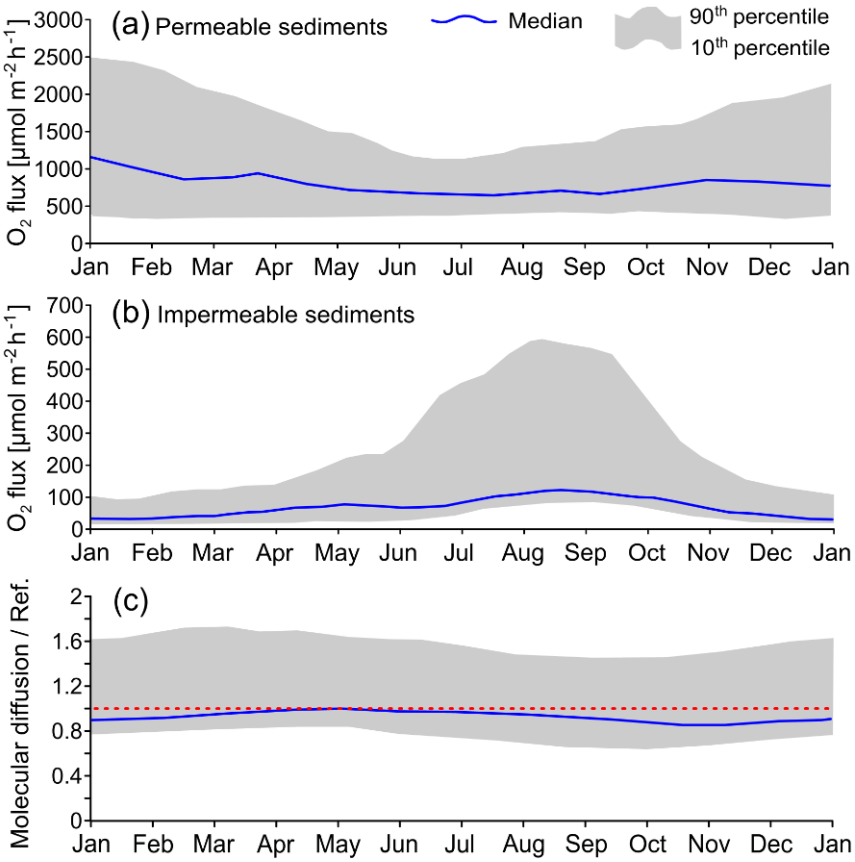

Figure 10. Simulated temporal (2012-2016) variation of (a) total oxygen flux across the sediment-water interface at the stations with permeable sediments (NOAH-A, NOAH-B, NOAH-E, CCP-G, NOAH-I) in No_D_b, (b) total oxygen flux at the stations with impermeable sediments (NOAH-C, NOAH-D, NOAH-F, NOAH-H) in No_D_b, and (c) ratio of molecular diffusive flux in No_D_b to the reference result at all stations. Note that the large range between the 10th and the 90th percentiles in the plots is attributed mainly to spatial variation among the stations.

3.2.6. Impact of bedform morphodynamics on oxygen flux

An important modulation of the oxygen flux across the sediment-water interface by small-scale bedform migration has been demonstrated in a numerical study by Ahmerkamp et al. (2015). Based on their results, Ahmerkamp et al. (2015) proposed three modes of porewater advection in permeable sediments: 1) Mode 1 corresponds to deep oxygen penetration and high oxygen flux when bedform is stationary, 2) Mode 2 refers to the formation of a redox seal during a competition of bedform migration and porewater flow ($0.01 < c_{ph}/u_p < 6$) that leads to a decreasing oxygen flux along with increasing bottom current velocity , and 3) Mode 3 represents a large reduction in the oxygen flux due to rapid

bedform migration ($c_{ph}/u_p > 6$) that overwhelms porewater flow. These modes were later confirmed by field observation in the German Bight (Ahmerkamp et al., 2017).

Our study further explores the impact of small-scale morphodynamics on oxygen flux at a longer time scale (2012-2016) based on 3-D hydrodynamic-biogeochemical modelling. To assess the impact of morphodynamics, a new simulation (termed No_Mor hereafter) with exclusion of bedform migration (i.e. c_{ph} is fixed to zero) was done, and results are compared with the reference result.

Simulation results indicate enhanced porewater advection in permeable sediments (Figure 11a) in No_Mor when compared to the reference result (Figure 6b). The ratio of the simulated porewater advective flux in No_Mor to the reference results is persistently larger than one in all seasons, with highest value in the cold season from November to February characterized by a 90% percentile up to 6 and a median larger than 1.4 (Figure 11b). These results suggest that actively migrating small-scale bedforms such as ripples and dunes effectively dampen oxygen input into sediments. Exclusion of such impact in numerical modelling or incubation chamber measurements would lead to an overestimation of the oxygen flux by nearly an order of magnitude in migrating bedforms. This is especially true for the shallow southern North Sea in the cold season (from October to February) when currents are driven by strong westerly winds often accompanied by storms (Sündermann and Pohlmann, 2011; Zhang et al., 2011; Geyer, 2014).

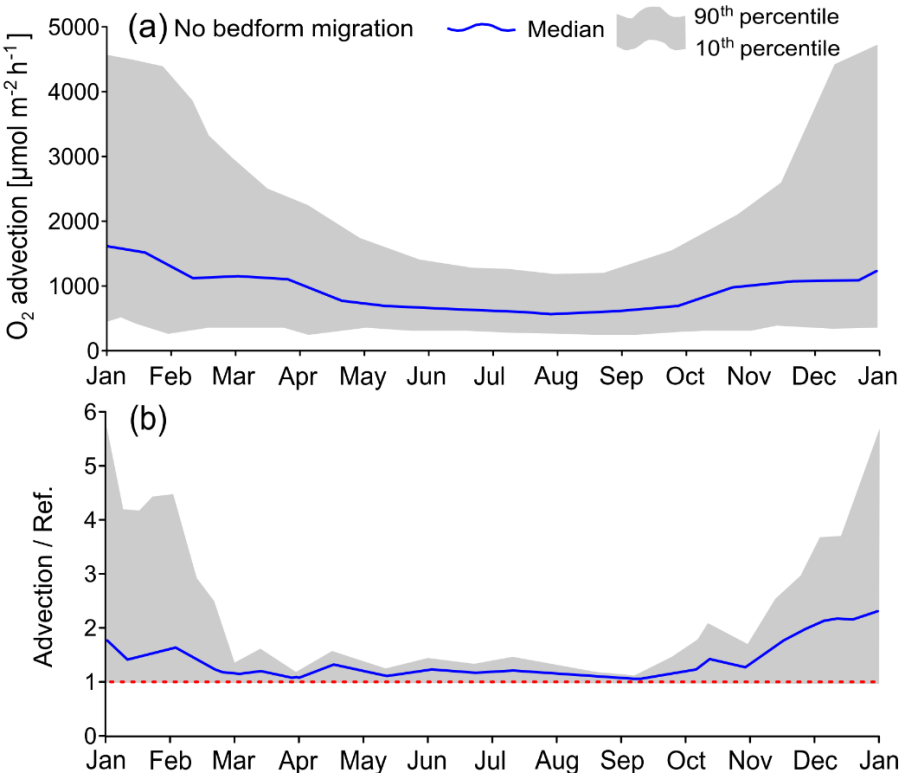

Figure 11. Simulated temporal (2012-2016) variation of (a) advective oxygen flux across the sediment-water interface at the stations with permeable sediments (NOAH-A, NOAH-B, NOAH-E, CCP-G, NOAH-I) in No_Mor, and (b) the ratio of advective oxygen flux in No_Mor to the reference result at these stations. Note that the large range between the 10th and the 90th percentiles in the plots is attributed mainly to spatial variation among the stations.

4. Discussion

4.1. Comparison with existing literature and research needs

The central importance of bioturbation in reworking of solids (POC) in coastal sediments at a regional scale has been demonstrated in Zhang et al. (2019), who showed that macrobenthos is able to rework more than 50% of the total budget of POC in the uppermost 30 cm sediments annually in the southern North Sea. The authors found that bioturbation diffusivity of solids in general ranges between 4×10^{-4} and 3×10^{-2} $cm^2\,h^{-1}$ with a mean value of 4.6×10^{-3} $cm^2\,h^{-1}$ in the study area. Rapid deposition of fresh POC in late Spring/early Summer may cause a bioturbation enhancement by an order of magnitude locally. Bioturbation has an even more profound impact on solutes than on solids. Berg et al. (2001) found that bioturbation diffusivity of solutes is at least one order of magnitude larger than that of solids. Our simulation results indicate that bioturbation diffusivity of oxygen in general varies between

568 8×10^{-2} (the 10th percentile) and 5×10^{-1} $cm^2\,h^{-1}$ (the 90th percentile) among the sampling stations,
569 which is 15-100 times of the mean bioturbation diffusivity of POC and 5-20 times of the corresponding
570 molecular diffusivity at the same sites. This result is supported by existing literature. For example, by
571 measurements of surface sediments collected in a sub-tidal area off Helsingør (Denmark) using a large
572 incubation chamber, Wenzhöfer and Glud (2004) found that macrobenthos-mediated oxygen flux was
573 the dominant oxygen consumptions process accounting for up to 92% of the total oxygen flux.
574 Jørgensen and Parkes, R. J. (2010) attributed the diffusivity of solutes (sulfate, methane, DIC) measured
575 in surface sediments in an embayment of the North Sea (Limfjorden, northern Denmark), which was
576 0.36-0.72 $cm^2\,h^{-1}$ and being 30-50 fold higher than the corresponding molecular diffusivity, to bio-
577 diffusion/bio-ventilation. Sulfate measurements in sediments of Aarhus Bay (Denmark) by Thamdrup et
578 al. (1994) indicated that bio-diffusivity was ~10^3 times higher than molecular diffusivity. In the mud
579 depocenter off Helgoland, the large spatial variations of benthic oxygen flux (up to a factor of 4) over
580 small distances was also attributed to macrobenthos (Oehler et al., 2015).

581 By inverse modelling using time series of measured benthic oxygen consumption rate, water-
582 column and sediment chlorophyll concentrations, and bottom water temperature at a fixed site off the
583 Belgian coast in the southern North Sea, Provoost et al. (2013) identified organic matter (POC) content
584 and temperature as two dominant controlling factors of oxygen flux across the sediment-water interface.
585 The impact of porewater advection was not taken into account because the measurements were done ex
586 situ. Therefore, their data represent diffusive fluxes only. The measured sediment oxygen uptake rate
587 ranged from 170 to 1340 $\mu mol\ m^{-2}\ h^{-1}$ (i.e. 4 to 32 $mmol\ m^{-2}\ d^{-1}$). Between January and March, the
588 lowest values were found, while the highest values were from summer between mid-June and mid-
589 August. Our results are consistent with these findings in terms of the magnitude and the seasonal
590 variation pattern. However, in their model Provoost et al. (2013) did not explicitly consider the effect of
591 macrobenthos on the oxygen flux, despite of quite abundant macrobenthos (ranging from 5.7 g C m^{-2} in

February to 78 g C m^{-2} in October) that potentially acted as an important mediator for transport of organic matter into the sediments at the sampling site. The impact of macrobenthos was instead implicitly incorporated in the sedimentary POC content since macrobenthos actively processes and transports POC into deeper sediments, thereby slowing down the degradation efficiency of POC (Meile and Van Cappellen, 2005; Middelburg, 2018; Zhang et al., 2019). This explains why the modelled degradation rate of POC was ~ $5.7 \pm 2.2 \times 10^{-3}$ d^{-1} in Provoost et al. (2013), which represents a typical value for semi-labile POC (Zhang et al., 2017) but is one order of magnitude smaller than that of labile POC originated from freshly deposited phytoplanktonic detritus (Westrich and Bemer, 1984; Harvey et al., 1995; Zhang et al., 2017). The critical importance of macrobenthos in mixing POC into sediments has been observed in various stations along the southern North Sea coast (e.g. Kamp and Witte, 2005; Le Guitton et al., 2017). Therefore, the importance of POC availability and bottom water temperature on the benthic oxygen flux are widely acknowledged (e.g. Glud, 2008; Provoost et al., 2013; Belley et al., 2016), while the impact of macrobenthos remains either implicit or mostly focused on small-scale experiments (Middelburg, 2018). This points out a need for quantitative assessment of the impact of bioturbation on benthic oxygen flux, especially at a regional to global scale. The benthic-pelagic coupled model system presented in this study, which explicitly resolves the interactions among benthic fauna, oxygen consumption and early diagenesis of POC, may serve as a useful tool to help address this issue.

4.2. Practical environmental indicators for benthic oxygen flux

It is widely acknowledged that benthic oxygen flux is highly variable in heterogeneous coastal seas and is affected by multiple factors including bottom water oxygen concentration, POC availability, temperature, light, hydrodynamics, sediment composition, sedimentation rates, and benthic fauna (Glud, 2008). The extent to which each factor contributes to the benthic oxygen flux depends on site characteristics and time of measurement (Belley et al., 2016; Chipman et al., 2016).

Our results at a regional scale (Figure 8) indicate that two environmental variables, namely d_{50} and macrobenthos biomass, can be particularly useful to identify hotspots of benthic oxygen flux. These two variables are highly correlated with other environmental factors such as hydrodynamics, temperature and POC availability, and can be used as proxies for these factors. For instance, on a sandy permeable seafloor, d_{50} is an indicator of hydrodynamics. A larger d_{50} implies stronger bottom currents and larger permeability, thereby facilitating stronger porewater flow and deeper oxygen penetration depth (Ahmerkamp et al., 2017). On the other hand, a fast migrating bedform (usually composed of fine sands) inhibits porewater advection and oxygen flux. This indicates that benthic oxygen flux on a sandy permeable seafloor may not be linearly related to d_{50} until d_{50} reaching a certain level. Our simulation results indicate that $d_{50} = 250$ μm defines such level and hotspots of benthic oxygen flux associated with porewater advection mostly occurs where $d_{50} \geq 250$ μm. Further investigations are nevertheless needed to judge whether this is valid and can be applied to other coastal regions.

Large variations of benthic oxygen flux over small distances on a homogeneous seafloor are often attributed to difference in benthic fauna through bioturbation (Oehler et al., 2015). However, since bioturbation is difficult to measure in field (Queirós et al., 2013; Griffiths et al., 2017; Middelburg, 2018), we propose to use macrobenthos biomass, which is easy to measure in field, as a practical indicator for hotspots of benthic oxygen flux because most hotspots associated with bio-diffusion are confined in the 5 g C m^{-2} biomass contour according to our results. Macrobenthos biomass is a proxy for POC quantity and quality (Dauwe et al., 1998; Herman et al., 1999; Campanyà-Llovet et al., 2017) which are jointly determined by hydrodynamics, primary production, temperature and sedimentation rate (Zhang and Wirtz, 2017). The community structure of macrobenthos, e.g. whether surface-feeding or subsurface-feeding communities dominate, imposes further control on the magnitude of benthic oxygen flux. Our results show that in the muddy hotspots the diffusive flux is mainly contributed by deposit feeders while in the sandy hotspots it is mainly caused by surface feeding animals including

suspension and filter feeders. The difference in community structure may explain the spatial heterogeneity of the magnitude of benthic oxygen flux within the hotspots (Figure 8d). However, since this argument is based on modeling results, further experimental work is needed to unravel a quantitative difference in benthic oxygen flux induced by different community structures, especially under the same setting of biomass.

5. Conclusions

Through an integrated study combining field observation and numerical modelling of the southern North Sea as an example, we have demonstrated the central importance of benthic animals in controlling benthic-pelagic coupling through mediating both solutes (oxygen) and solids (POC) transport across the sediment-water interface. The following conclusions are drawn.

Both advective and diffusive oxygen fluxes across the sediment-water interface are characterized by strong seasonality in the study area. However, the variation pattern and driving mechanisms behind them are different. Variation of the advective flux is a summer-low, winter-high pattern mainly driven by hydrodynamics and bedform morphodynamics, while variation of the diffusive flux is summer-high and winter-low resulting from a combined effect of pelagic drivers (hydrodynamics, temperature and primary production) and benthic dynamics associated with the interaction between organic carbon and macrobenthos.

In permeable sediments, a combination of the opposite seasonal varying patterns of advection and diffusion results in large spatial and temporal variability among individual sites at a local scale but a consistent and mild seasonal variation (summer-high and winter-low) at a regional scale. In impermeable sediments, benthic oxygen fluxes are dominated by bio-diffusion exhibiting a remarkable seasonality. Local-scale spatial and temporal variability there is mainly caused by availability of POC originated from freshly deposited phytoplankton detritus and subsequent bioturbation intensity of macrobenthos related to food-foraging and growth.

663 Bio-diffusion caused by macrobenthos contributes to more than 85% and 52% of the total benthic
664 oxygen fluxes in muddy seabed and at a regional scale, respectively.

665 Last but not least, we found two environmental variables, namely d_{50} and macrobenthos biomass,
666 that can be particularly useful for identifying hotspots of benthic oxygen fluxes in coastal shelf
667 environments.

668 ***References***

669 Ahmerkamp, S., C. Winter, F. Janssen, M. M. M. Kuypers, and M. Holtappels. 2015. The impact of
670 bedform migration on benthic oxygen fluxes. J. Geophys. Res. 120: 2229–2242,
671 doi:10.1002/2015JG003106

672 Ahmerkamp, S., Winter, C., Krämer, K., Beer, D.d., Janssen, F., Friedrich, J., et al. 2017. Regulation of
673 benthic oxygen fluxes in permeable sediments of the coastal ocean. Limnol Oceanogr 62: 1935– 1954.

674 Aquino, T., Roche, K. R., Aubeneau, A., Packman, A. I., and Bolsterm, D. 2017. A process-based model
675 for bioturbation-induced mixing. Scientific Reports, 7(1), 14287. https://doi.org/10.1038/s41598-017-
676 14705-1

677 Becker, G. A., Giese, H., Isert, K., König, P., Langenberg, H., Pohlmann, T., and Schrum, C.1999.
678 Mesoscale structures, fluxes and water mass variability in the German Bight as exemplified in the
679 KUSTOS-experiments and numerical models, German Journal of Hydrography, 51, 55–179,
680 doi:10.1007/BF02764173

681 Belley, R. and Snelgrove, P.V.R. 2016. Relative contributions of biodiversity and environment to
682 benthic ecosystem functioning. Front. Mar. Sci. 3, 242, doi: 10.3389/fmars.2016.00242

683 Belley, R., Snelgrove, P. V. R., Archambault, P., and Juniper, S. K. 2016. Environmental drivers of
684 benthic flux variation and ecosystem functioning in Salish Sea and Northeast Pacific sediments. PLoS
685 ONE 11:e0151110, doi: 10.1371/journal.pone.0151110

686 Berg, P., Rysgaard, S., Funch, P., and Sejr, M. 2001. Effects of bioturbation on solutes and solids in
687 marine sediments: Aquatic Microbial Ecology 26, 81–94.
688 Berner, R. A. 1980. In N. J. Princeton (Ed.), Early diagenesis: A theoretical approach. Princeton series
689 in geochemistry (p. 241). Princeton: Princeton University Press.
690 Boudreau, B. P. 1986a. Mathematics of tracer mixing in Sediments: I. Spatially-dependent, diffusive
691 mixing. Am. J. Sci. 286: 161–198.
692 Boudreau, B. P. 1986b. Mathematics of tracer mixing in sediments. II. Nonlocal mixing and biological
693 conveyor belt phenomena. Am. J. Sci. 286: 199−238.
694 Brown, J.H., Gillooly, J.F., Allen, A.P., Savage, V.M., West, G.B. 2004. Toward a metabolic theory of
695 ecology. Ecology, 85: 1771–1789.
696 Butensch ön, M., Clark, J., Aldridge, J. N., Allen, J. I., Artioli, Y., Blackford, J., et al. 2016. ERSEM
697 15.06: a generic model for marine biogeochemistry and the ecosystem dynamics of the lower trophic
698 levels. Geosci. Model Dev. 9: 1293–1339, doi:10.5194/gmd-9-1293-2016
699 Campany à-Llovet, N., Snelgrove, P. V. R., and Parrish, C. C. 2017. Rethinking the importance of food
700 quality in marine benthic food webs. Progress in Oceanography 156, 240-251.
701 https://doi.org/10.1016/j.pocean.2017.07.006.
702 Cardinale, B.J. and Palmer, M.A. 2002. Species diversity enhances ecosystem functioning through
703 interspecific facilitation. Nature 415, 426–429.
704 Chen, C. A., and Borges, A. V. 2009. Reconciling opposing views on carbon cycling in the coastal
705 ocean: Continental shelves as sinks and near-shore ecosystems as sources of atmospheric CO2. Deep
706 Sea Research Part II: Topical studies in Oceanography, 56(8-10), 578–590, doi:
707 10.1016/j.dsr2.2009.01.001.
708 Chipman, L., Berg, P., and Huettel, M. 2016. Benthic oxygen fluxes measured by eddy covariance in
709 permeable Gulf of Mexico shallow-water sands. Aquatic Geochemistry, 22, 529–554.

710 Ciais, P., Sabine, C., Bala, G., Bopp, L., Brovkin, V., Canadell, J., et al. 2013. "Carbon and other
711 biogeochemical cycles," in Climate Change 2013: ThePhysical Science Basis Contribution of
712 Working Group I to theFifth Assessment Report of the Intergovernmental Panel on Cli-mate Change,
713 edited by: Stocker, T., Qin, D., Plattner, G.-K., Tig-nor, M., Allen, S., Boschung, J., Nauels, A., Xia,
714 Y., Bex, V., and Midgley, P., Cambridge University Press, Cambridge, UK and New York, NY, USA,
715 465–570.
716 Cloern, J. E., Abreu, P. C., Carstensen, J., Chauvaud, L., Elmgren, R., Grall, J., et al. 2016. Human
717 activities and climate variability drive fast-paced change across the world's estuarine-coastal
718 ecosystems. Global Change Biology, 22, 513–529, doi:10.1111/gcb.13059.
719 Daewel, U., and Schrum, C. 2013. Simulating long-term dynamics of the coupled North Sea and Baltic
720 Sea ecosystem with ECOSMO II: Model description and validation. Journal of Marine Systems, 119–
721 120, 30–49. https://doi.org/10.1016/j.jmarsys.2013.03.008
722 Dauwe, B., Herman, P. M. J., Heip, C. H. R. 1998. Community structure and bioturbation potential of
723 macrofauna at four North Sea stations with contrasting food supply. Marine Ecology Progress Series
724 173, 67–83. https://doi.org/10.3354/meps173067
725 Elliott, A. H., and Brooks, N. H. 1997. Transfer of nonsorbing solutes to a streambed with bed
726 forms:Theory. Water Resources Research, 33(1), 123–136.
727 Falkowski, P., Scholes, J. R., Boyle, E., Canadell, J., Canfield, D., Elser, J., et al. 2000. The global
728 carbon cycle: a test of our knowledge of earth as a system. Science 290, 291–296. doi:
729 10.1126/science.290.5490.291
730 Gattuso, J. P., Frankignoulle, M., Wollast, R. 1998. Carbon and carbonate metabolism in coastal aquatic
731 ecosystems. Annual Reviews of Ecological Systems 29, 405–434.
732 Geyer, B. 2014. High-resolution atmospheric reconstruction for Europe 1948–2012: coastDat2. Earth
733 Syst. Sci. Data 6 (1), S. 147–164.

734 Glud, R. N. 2008. Oxygen dynamics of marine sediments. Marine Biology Research 4(4), 243-289.
735 doi:10.1080/17451000801888726
736 Griffiths, J. R., Kadin, M., Nascimento, F. J. A., Tamelander, T., Tonroos, A., Bonaglia, S., et al. 2017.
737 The importance of benthic-pelagic coupling for marine ecosystem functioning in a changing world.
738 Global Change Biology 23, 2179−2196. doi: 0.1111/gcb.13642 2017
739 Harvey, H., Tuttle, J., Bell, J., 1995. Kinetics of phytoplankton decay during simulated sedimentation:
740 changes in biochemical composition and microbial activity under oxic and anoxic conditions.
741 Geochimica et Cosmochima Acta 59, 3367−3377.
742 Hedges, J.I., Baldock, J.A., Gélinas, Y., Lee, C., Peterson, M.L., Wakeham, S.G. 2002. The biochemical
743 and elemental compositions of marine plankton: a NMR perspective. Mar Chem 78:47–63.
744 Heinze, C., Meyer, S., Goris, N., Anderson, L., Steinfeldt, R., Chang, N., et al. 2015. The ocean carbon
745 sink - impacts, vulnerabilities and challenges. Earth Syst. Dynam. 6, 327-358. doi:10.5194/esd-6-327-
746 2015
747 Herman, P. M. J., Middelburg, J. J., Van de Koppel, J., and Heip, C. H. R. 1999. The ecology of
748 estuarine macrobenthos. Advances in Ecological Research 29, 195–240.
749 https://doi.org/10.1016/S0065-2504(08)60194-4
750 Holstein, J. M., and Wirtz, K. W. 2009. Sensitivity analysis of nitrogen and carbon cycling in marine
751 sediments. Estuarine, Coastal and Shelf Science, 82(4), 632-644.
752 Hülse, D., Arndt, S., Daines, S., Regnier, P., and Ridgwell, A. 2018. OMEN-SED 1.0: a novel,
753 numerically efficient organic matter sediment diagenesis module for coupling to Earth system models.
754 Geosci. Model Dev., 11, 2649–2689. doi:10.5194/gmd-11-2649-2018
755 Jørgensen, B. B., and Parkes, R. J. 2010. Role of sulfate reduction and methane production by organic
756 carbon degradation in eutrophic fjord sediments (Limfjorden, Denmark). Limnology and
757 Oceanography 55(3), 1,338–1,352. https://doi.org/10.4319/lo.2010.55.3.1338

Kamp, A., and Witte, U. 2005. Processing of 13C-labelled phytoplankton in a fine-grained sandy-shelf sediment (North Sea): relative importance of different macrofauna species. Marine Ecology Progress Series, 297, 61–70. https://doi.org/10.3354/meps297061

Kelly-Gerreyn, B. A., Martin, A. P., Bett, B. J., Anderson, T. R., Kaariainen, J. I., Main, C. E., et al. 2014. Benthic biomass size spectra in shelf and deep-sea sediments. Biogeosciences, 11, 6401–6416.

Krämer, K., and C. Winter. 2016. Predicted ripple dimensions in relation to the precision of in situ measurements in the southern North Sea. Ocean Sci. 12: 1221–1235. doi: 10.5194/os-12-1221-2016

Le Guitton, M., Soetaert, K., Damste, J.S.S., Middelburg, J. J. 2017. A seasonal study of particulate organic matter composition and quality along an offshore transect in the southern North Sea. Estuarine, Coastal and Shelf Science 188, 1−11.

Le Quéré, C., Andrew, R. M., Friedlingstein, P., Sitch, S., Pongratz, J., Manning, A. C., et al. 2018. Global carbon budget 2017. Earth System Science Data 10, 405–448. https://doi.org/ 10.5194/essd-10-405-2018

Lohrer, A.M., Thrush, S. F., and Gibbs, M. M. 2004. Bioturbators enhance ecosystem function through complex biogeochemical interactions. Nature 431, 1092–1095. doi:10.1038/nature03042

Maerz, J., Hofmeister, R., van der Lee, E.M., Gräwe, U., Riethmüller, R., and Wirtz, K.W. 2016. Maximum sinking velocities of suspended particulate matter in a coastal transition zone. Biogeosciences 13, 4863–4876.

Meile, C., and Van Cappellen, P. 2005. Particle age distributions and O2 exposure times: timescales in bioturbated sediments. Global Biogeochem. Cycles 19:GB3013. doi: 10.1029/2004GB002371

Meysman, F. J. R., Boudreau, B. P., and Middelburg, J. J. 2003. Relations between local, nonlocal, discrete and continuous models of bioturbation. Journal of Marine Research, 61(3), 391–410. https://doi.org/10.1357/002224003322201241

Meysman, F. J. R., J. J. Middelburg, and C.H.R. Heip. 2006b. Bioturbation: a fresh look at Darwin's last idea. Trends Ecol. Evol. 21: 688–695. doi: 10.1016/j.tree.2006.08.002

783 Meyer, J., Nehmer, P., Kröncke, I. 2019. Shifting south-eastern North Sea macrofauna bioturbation
784 potential over the past three decades: a response to increasing SST and regionally decreasing food
785 supply. Mar. Ecol. Prog. Ser. 609: 17–32.
786 Middelburg, J. J., and K. Soetaert. 2004. The role of sediments in shelf ecosystem dynamics. In K. H. B.
787 Allan and R. Robinson [eds.], The global coastal ocean. Harvard University Press. p. 353–375.
788 Middelburg, J. J. 2018. Reviews and syntheses: to the bottom of carbon processing at the seafloor.
789 Biogeosciences 15, 413–427. doi: 10.5194/bg-15-413-2018
790 Muller-Karger, F. E., Varela, R., Thunell, R., Luerssen, R., Hu, C., and Walsh, J. J. 2005. The
791 importance of continental margins in the global carbon cycle. Geophysical Research Letters 32,
792 L01602, doi:10.1029/2004GL021346
793 Neumann, A., Möbius, J., Hass, H. C., Puls, W., and Friedrich, J. 2017. Empirical model to estimate
794 permeability of surface sediments in the German Bight (North Sea). Journal of Sea Research, 127, 36-
795 45. https://doi.org/10.1016/j.seares.2016.12.002
796 Neumann, A., Hass, C. H., Möbius, J., and Naderipour C. 2019. Ballasted flocs capture pelagic primary
797 production and alter the local sediment characteristics in the coastal German Bight (North Sea).
798 Geosciences 9(8), 344, doi: 10.3390/geosciences9080344
799 Nihoul, J. C. J. 1980. Residual circulation, long waves and mesoscale eddies in the North Sea. Oceanol.
800 Acta. 3 (3): 309-316.
801 Oehler, T., Martinez, R., Schückel, U., Winter, C., Kröncke, I., Schlüter, M., 2015. Seasonal and spatial
802 variations of benthic oxygen and nitrogenfluxes in theHelgoland Mud Area (southern North Sea).
803 Cont. Shelf Res. 106, 118–129.
804 Pearson, T. H., and Rosenberg, R. 1987) Feast and famine: Structuring factors in marine benthic
805 communities. In The 27th Symposium of the British Ecological Society, eds. J. H. R. Gee, and P. S.
806 Giller (Aberystwyth, Oxford: Blackwell Scientific Publications), 373–395.

Provoost, P., Braeckman, U., Van Gansbeke, D., Moodley, L., Soetaert, K.,Middelburg, J.J., Vanaverbeke, J. 2013. Modelling benthic oxygen consumption and benthic-pelagic coupling at a shallow station in the southern North Sea. Estuar. Coast. shelf Sci. 120, 1–11. http://dx.doi.org/10.1016/j.ecss.2013.01.008

Queirós, A. M., Birchenough, S. N. R., Bremner, J., Godbold, J. A., Parker, R. E., Romero‐Ramirez, A., et al. 2013. A bioturbation classification of European marine infaunal invertebrates. Ecology and Evolution, 3(11), 3958–3985. https://doi.org/10.1002/ece3.769

Queirós, A. M., Stephens, N., Cook, R., Ravaglioli, C., Nunes, J., Dashfield, S., et al. 2015. Can benthic community structure be used to predict the process of bioturbation in real ecosystems? Prog. Oceanogr. 137, 559–569. doi: 10.1016/j.pocean.2015.04.027

Santos, I. R., D. Eyre, and M. Huettel. 2012. The driving forces of porewater and groundwater flow in permeable coastal sediments: A review. Estuar. Coast. Shelf Sci. 98: 1–15. doi:10.1016/j.ecss.2011.10.024

Schiffers, K., Teal, L. R., Travis, J. M. J., Solan, M. 2011. An open source simulation model for soil and sediment bioturbation. PLOS ONE 6: e28028.

Schrum, C. 1997. Thermohaline stratification and instabilities at tidal mixing fronts: results of an eddy resolving model for the German Bight. Continental Shelf Research, 17(6), 689–716. https://doi.org/10.1016/S0278-4343(96)00051-9

Schrum, C., Alekseeva, I., and St. John, M. 2006a. Development of a coupled physical‐biological ecosystem model ECOSMO. Journal of Marine Systems, 61(1-2), 79-99. https://doi.org/10.1016/j.jmarsys.2006.01.005

Schrum, C., St. John, M., and Alekseeva, I. 2006b. ECOSMO, a coupled ecosystem model of the North Sea and Baltic Sea: Part II. Spatial seasonal characteristics in the North Sea as revealed by EOF analysis. Journal of Marine Systems, 61(1-2), 100-113. https://doi.org/10.1016/j.jmarsys.2006.01.004

831 Snelgrove, P. V. R., Soetaert, K., Solan, M., Thrush, S., Wei, C.-L., Danovaro, R., et al. 2018. Global
832 carbon cycling on a heterogeneous seafloor. Trends. Ecol. Evol. 33, 96–105. doi:
833 10.1016/j.tree.2017.11.004
834 Soetaert, K., Herman, P. M., Middelburg, J. J., Heip, C., de Stigter, H. S., van Weering, T. C., et al.
835 1996a. Modeling 210Pb-derived mixing activity in ocean margin sediments: diffusive versus nonlocal
836 mixing. J. Mar. Res. 54: 1207−1227.
837 Soetaert, K., P. M. J. Herman, and J. J. Middelburg. 1996b. A model of early diagenetic processes from
838 the shelf to abyssal depths. Geochim. Cosmochim. Acta 60: 1019–1040. doi: 10.1016/0016-
839 7037(96)00013-0
840 Soulsby, R. L., Whitehouse, R. J. S., and Marten, K. V. 2012. Prediction of time-evolving sand ripples
841 in shelf seas, Cont. Shelf Res., 38,47–62, doi: 10.1016/j.csr.2012.02.016
842 Stanev, E., M. Dobrynin, A. Pleskachevsky, S. Grayek, and H. Günther. 2009. Bed shear stress in the
843 southern North Sea as an important driver for suspended sediment dynamics. Ocean Dyn. 59(2):183–
844 194. doi: 10.1007/s10236-008-0171-4
845 Sündermann, J., and Pohlmann, T. 2011. A brief analysis of North Sea physics. Oceanologia, 53(3),
846 663–689. https://doi.org/10.5697/oc.53–3.663
847 Teal, L. R., Bulling, M. T., Parker, E. R., Solan, M. 2008. Global patterns of bioturbation intensity and
848 mixed depth of marine soft sediments. Aquatic Biology, 2, 207–218. doi: 10.3354/ab00052
849 Thamdrup, B., Fossing, H., and Jørgensen, B.B. 1994. Manganese, iron, and sulfur cycling in a coastal
850 marine sediment, Aarhus Bay, Denmark. Geochim. Cosmochim. Acta 58: 5115–5129,
851 doi:10.1016/0016-7037(94)90298-4
852 Ullman, W. J. and Aller, R. C. 1982. Diffusion coefficients in nearshore marine sediments, Limnol.
853 Oceanogr., 27, 552–556. doi: 10.4319/lo.1982.27.3.0552

van Beusekom, J. E. E., U. H. Brockmann, K.-J. Hesse, W. Hickel, K. Poremba, and U. Tillmann. 1999. The importance of sediments in the transformation and turnover of nutrients and organic matter in the Wadden Sea and German Bight. German J. Hydrogr. 51: 245–266.

Wenzhöfer, F., and Glud, R. N. 2004. Small-scale spatial and temporal variability in coastal benthic O_2 dynamics: effects of fauna activity. Limnol. Oceanogr., 49(5), 1471–1481.

Westrich, J. T., and Bemer, R. A. 1984. The role of sedimentary organic matter in sulfate reduction: The G-model testes. Limnology and Oceanography, 29, 236–249. https://doi.org/10.4319/lo.1984.29.2.0236

Whearcroft, R. A., Jumars, P. A., Smith, C. R., Nowell, A. R. M. 1990. A mechanistic view of particulate biodiffusion coefficient: Step lengths, rest periods and transport directions. Journal of Marine Research 48, 177–207.

Wollast, R. 1991. The coastal organic carbon cycle: fluxes, sources and sinks. In J.-M. M. R.-F.-C. Mantoura, R. Wollast [ed.], Ocean Margin Processes in Global Change. John Wiley & Sons, p. 365-381.

Zhang, W., Harff. J and Schneider, R. 2011. Analysis of 50-year wind data of the southern Baltic Sea for modelling coastal morphological evolution - a case study from the Darss-Zingst Peninsula. Oceanologia, 53 (1-TI), 489-518. doi:10.5697/oc.53-1-TI.489

Zhang, W., and Wirtz, K. 2017. Mutual dependence between sedimentary organic carbon and infaunal macrobenthos resolved by mechanistic modeling. Journal of Geophysical Research–Biogeosciences 122, 2509–2526. doi:10.1002/2017JG003909

Zhang, W., Wirtz, K., Daewel, U., Wrede, A., Kröncke, I., Kuhn, G., Neumann, A., Meyer, J., Ma, M., & Schrum, C. 2019: The budget of macrobenthic reworked organic carbon - a modelling case study of the North Sea. Journal of Geophysical Research-Biogeosciences 124(6), 1446–1471. doi:10.1029/2019JG005109

Acknowledgements

This study is a contribution to the I^2B project "Unravelling the linkages between benthic biological functioning, biogeochemistry and coastal morphodynamics – from big data to mechanistic modelling " funded by Helmholtz-Zentrum Geesthacht. Simulation results at the sampling stations and the source code of TOCMAIM with a coupling interface to 3-D hydrodynamic biogeochemical models are stored in Mendeley Data with open access at http://dx.doi.org/10.17632/2vvny3xd85.1.

Conflict of Interest

None declared.